2011-01-01

Modeling Impulse Oscillometry Data: Using Augmented-RIC and Extended-RIC Respiratory Impedance Model Paramaters to Track Pulmonary Health and Disease

Carlos Domingo Ramos Rocha
University of Texas at El Paso, c.ramos.rocha@gmail.com

MODELING IMPULSE OSCILLOMETRY DATA: USING AUGMENTED-RIC AND EXTENDED-RIC RESPIRATORY IMPEDANCE MODEL PARAMETERS TO TRACK PULMONARY HEALTH AND DISEASE

CARLOS D. RAMOS ROCHA

Department of Electrical and Computer Engineering

APPROVED:

_____
Homer Nazeran, Ph.D., Chair

_____
Joseph Pierluissi, Ph.D.

_____
Martine Ceberio, Ph.D.

_____
Jorge Ibarra, M.D, MPH

_____
Benjamin C. Flores, Ph.D
Acting Dean of Graduate School

To my mom, my dad, my sister and my brother.

Your love and encouragement give me strength.

MODELING IMPULSE OSCILLOMETRY DATA: USING AUGMENTED-RIC AND EXTENDED-RIC RESPIRATORY IMPEDANCE MODEL PARAMETERS TO TRACK PULMONARY HEALTH AND DISEASE

by

CARLOS D. RAMOS ROCHA, BSEE

THESIS

Presented to the Faculty of the Graduate School of

The University of Texas at El Paso

in Partial Fulfillment

of the Requirements

for the Degree of

MASTER OF SCIENCE

Department of Electrical and Computer Engineering

THE UNIVERSITY OF TEXAS AT EL PASO

August 2011

ACKNOWLEDGEMENTS

First and foremost I would like to thank my parents. They are with me in every decision I make. Their love and encouragement are the reasons behind every one of my accomplishments past, present and future. They have helped my every step of the way, pushing me forward with their wisdom and support and giving me strength when I've faltered, they are each the best person I know. I would also like to thank my brother and sister, for all your kind words and advise, for your unconditional love, but most of all for being my best friends.

I would like express my utmost gratitude to my advisor, Dr. Homer Nazeran. More than anyone else he is directly responsible for the pursuit and conclusion of my graduate studies. He believed in me enough to make me his research assistant and never lost confidence in me. His support, guidance and friendship were all instrumental in making this possible.

I'm especially grateful to the late, great Dr. Michael Goldman. He thought me most of what I know regarding subject of this thesis and his enthusiasm was a source of great inspiration. He was one of the smartest people I will ever meet but more importantly, also one of the kindest. I greatly admired him and yet he never made me feel like anything less than his peer. I only hope he would be proud of this work.

This study was made possible in large part thanks to the generous contribution of information from many distinct sources. It's not possible for me to name here every single person that was involved but they all have my most sincere gratitude.

And finally, I would like to thank my friends. I'm fortunate to have some of the most loyal, selfless, kind and patient people among my closest friends, and I consider them to be my

extended family. They have always been with me in my time of need, especially in this last year. To name them here is unnecessary; yet this work would not have been possible without them.

ABSTRACT

Respiratory diseases are a great health concern. Early detection of disease could greatly improve quality of life and yet the most common pulmonary function test can be an unreliable diagnostic method, especially in the case of children. A reliable method of detecting and assessing small airway impairment could greatly help with timely diagnosis. This research approaches this problem by taking Impulse Oscillometry (IOS) data and its model-derived parameters and assessing their using in tracking respiratory function and more specifically, small airway function.

This research first describes the use of electric circuits as models to describe lung properties at distinct regions of the respiratory system. Analyzing one of the most successful of these models, Mead's respiratory impedance model, it was concluded that it was inappropriate when using IOS data. It is reasoned that the very small volume displacements generated with this testing technique do not sufficiently stimulate the subjects' lung tissue and chest wall making two parameters found in Mead's model irrelevant. Therefore the augmented-RIC (aRIC) and extended-RIC (eRIC) models are proposed as more suitable respiratory impedance models for IOS data.

In order to estimate model parameters an algorithm was developed based on the nonlinear least squares minimization technique. A very large and diverse database was obtained consisting of 670 IOS test results from patients classified as normal (NL), asthmatic (ASTH) or small airway impaired (SAI). Using the developed algorithm and database model parameters were estimated for both the aRIC and eRIC models. It was found that both models succeeded almost

equally well in modeling IOS data providing good data fit for all data classifications (NL, ASTH or SAI).

Statistical analysis showed that model-derived parameters are able to discriminate between health and disease while at the same time monitoring response to bronchodilator administration, with the peripheral compliance (C_p) model parameter showing an even better response than IOS-derived indices.

The use of such a large database makes it possible for this study to provide a reliable range of what can be considered to be "normal" values for IOS indices, which can be used by themselves as useful indices of small airway impairment. However, it is concluded that model-derived parameters work equally well in differentiating health from disease while providing insight into the function of specific lung regions. This is especially true in the case of the aRIC model, which tracks lung function in a reliable and realistic manner.

CONTENTS

Page

LIST OF TABLES

LIST OF FIGURES

Chapter 1: INTRODUCTION

1.1 PROBLEM STATEMENT

If all respiratory diseases are lumped together they account for one third of the annual deaths in the US (1). Some of the most common respiratory diseases such as asthma, chronic obstructive pulmonary disease (COPD) and emphysema can be hard to diagnose for several reasons such as similarities to other diseases and the lack of reliable testing. For example, asthma affects 7.7% of adults and 9.6% of children in the US (2), yet it can be misdiagnosed as hay fever, cardiac problems or infection. Accurate diagnosis is especially problematic in children because the most common testing methods lack reliable indices unless the disease is particularly aggravated (3).

Forced Oscillation Technique (FOT) is a testing method which can be used to determine mechanical properties of the respiratory system (4) and hence, assess pulmonary function. While conventional methods measure respiratory function using forced breathing maneuvers, FOT does so by superimposing external air pressures on a subject's normal tidal breathing, requiring only passive cooperation from said subject. These external pressures are then used to determine the total mechanical *impedance* created by the airways.

Since its beginnings the main hurdle for FOT has always seemed to be the lack of consensus on a practical and intuitive way of applying and interpreting the obtained results. This potential problem was recognized early on, and in an attempt to curb this obstacle the use of models representing human airways was introduced (5). However, over the years FOT has simultaneously developed along different paths varying in their use of, among other things, different excitation signals and frequency ranges; because of this, many models have now been developed and used.

Some research on this topic focuses on using simple models containing only physiologically realistic components that are useful in clinical diagnosis (4)-(10). Other research may use varied

frequency ranges, several oscillatory signals or combinations of several methods (such as FOT with plethysmography). Many studies very often strive to create models that fit data as accurately as possible and there seems to be a trend towards increasing complexity: there are models taking into account gas compressibility (11), (12), admittance as an independent parameter (13), alveolar and pleural pressures (14), there are also fractional-order models (15) and those that use a very large number of parameters (16), among others.

While the existence of such a rich variety of studies has provided much evidence to the fact that FOT is very useful in the assessment of respiratory function, the use of model-based parameters as a diagnostic tool is still not yet widely accepted.

1.2 PROPOSED SOLUTION

In order for FOT model-derived parameters to be useful in clinical settings as a diagnostic tool they must provide reliable, intuitive and relevant results that are easy to understand and interpret by healthcare professionals. In order for an impedance model to be adequate for such task it ought to be versatile enough to provide very good data fit regardless of a subject's pulmonary health, providing physiologically-significant parameters with realistic values and preferably it should be simple and straightforward enough to understand by healthcare professionals and the patient's tested.

Since its conception, Mead's respiratory impedance model (4) has shown to be very good at modeling data obtained from subjects with many types of respiratory conditions while using only parameters that are relevant airway impairment diagnosis. Via a (relatively) small number of parameters it is able to represent properties for upper respiratory tract, small airways and account for elasticity of the cheeks.

Although the advantages of this model are widely acknowledged this study will provide evidence that simplified versions of it, the augmented-RIC (aRIC) model and the extended-RIC (eRIC) model,

provide all the same benefits while reducing its complexity and increasing the physiological significance of the obtained values for those remaining parameters.

This thesis is organized into ten chapters. Chapter 2 provides a summary of concepts necessary to understand this research including the human respiratory system's anatomy and physiology, the mechanics of breathing and its properties, respiratory function tests, respiratory impedance and some relevant pulmonary diseases. Chapter 3 provides technical background on the Impulse Oscillometry System (IOS) used to acquire data for this study. Chapter 4 gives an in-depth look at several respiratory impedance models, their background, theory and parameters. Chapter 5 deals with model parameter estimation, some theory of numerical optimization and describes the optimization algorithm developed as part of this research. Chapter 6 describes the patient database used in this study, how patients were classified according to pulmonary health and the measures taken to assure good data quality. Chapter 7 reviews parameter estimation results for several models and several diseases, summarizes modeling errors and discusses Mead's model main disadvantage when compared to the aRIC and eRIC models. Chapter 8 is a detailed analysis of Mead's model and how it behaves when used to model IOS data, it then goes on to provide justification for using simpler models. Chapter 9 talks about the use of model-derived parameters as tools for detecting pulmonary disease, how those parameters relate to IOS indices of airway function and whether or not the parameters themselves are able to distinguish healthy from diseased lungs. Finally, chapter 10 summarizes all of the results and discusses the merits of using IOS in conjunction with these model-derived parameters to assess pulmonary function and more importantly the possibility of using this method as reliable, sensitive and practical alternative to conventional pulmonary function testing methods.

Chapter 2: THE HUMAN RESPIRATORY SYSTEM

Respiration refers to the gas exchange that occurs between the living body and its surrounding environment. Breathing-in and breathing-out is a very complicated process which requires the proper condition, functioning and interaction of many organs in order to efficiently provide the vital oxygen needed in the body's ever-changing internal environment, while simultaneously eliminating poisonous carbon dioxide from the cells.

Breathing mechanics and its underlying properties are key concepts necessary in understanding respiratory impedance, its relation to pulmonary function and in general, the research presented here. As such, this chapter provides a brief review of the anatomy and physiology of the human respiratory system, the mechanics of breathing, testing methods currently used in assessing pulmonary function and relevant pulmonary diseases.

2.1 ANATOMY OF THE HUMAN RESPIRATORY SYSTEM

The body's respiratory system can be divided anatomically into upper and lower respiratory tracts. The *upper respiratory tract* includes the nose, nasal cavity, mouth, pharynx, larynx and trachea. The *lower respiratory tract* includes the lungs; inside the lungs are the bronchi, bronchioles and alveoli. Also part of the respiratory system is the diaphragm, a muscle which by its contraction and relaxation makes inspiration and expiration possible. Figure 2-1 (17) depicts these major organs involved in respiration.

Gas exchange occurs within the lungs in what is commonly known as the *airway tree*, it starts with the trachea and then branches into two bronchi, one for each lung, each bronchus continues to branch eventually forming bronchioles. Each airway branching is considered a new generation; the first seventeen generations are the *conducting zone*. Actual gas exchange occurs in the last seven generations of airway branches, the *respiratory zone.* This zone is made up mostly of alveoli and alveoli ducts. Lungs

themselves are contained within the chest cavity while not actually attached to it; there is thin layer of *pleural fluid* constantly separating the cavity wall from the lung tissue (18).

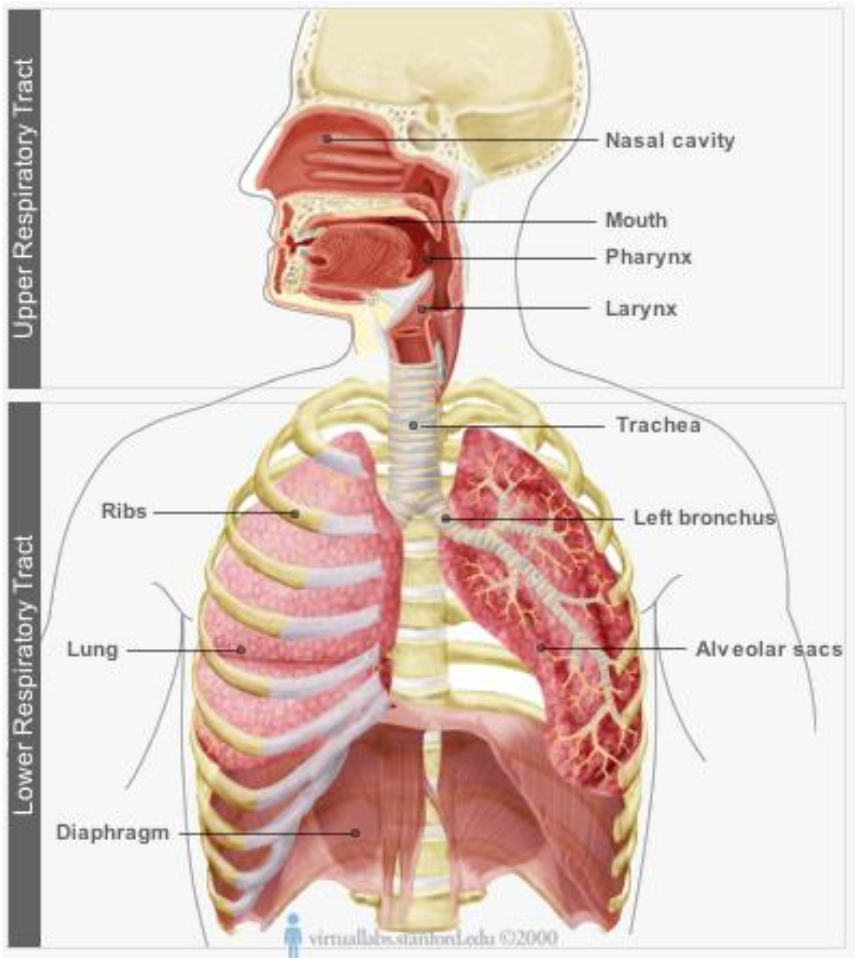

Figure 2-1: The human respiratory system can be divided into two tracts. The upper respiratory tract is formed by the mouth, nasal cavity, pharynx and larynx; the lower respiratory tract starts at the trachea and contains the ribs, diaphragm and the lungs including the airway passages such as the bronchi, bronchioles and alveoli.

2.2 PHYSIOLOGY OF THE HUMAN RESPIRATORY SYSTEM

Gas exchange occurs in the respiratory zone where alveoli and their ducts merge with pulmonary capillaries forming a very thin *blood-gas interface*. Alveoli, shown in Figure 2-2 (19), are like small pockets emerging from alveolar ducts providing a great increase in surface area: a typical adult lung has

around 300 million alveoli providing a total surface area of around 75 m^2, 70% to 80% of which is covered with pulmonary capillaries (18).

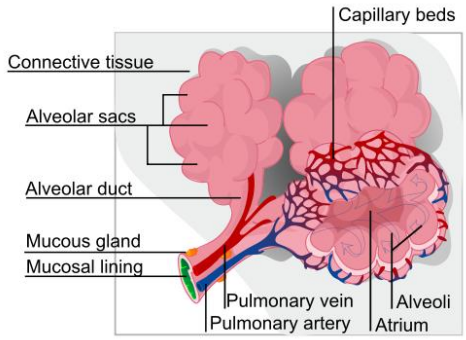

Figure 2-2: Alveoli are the site of gas exchange, they are mostly covered in capillary beds and at this point there is only a very thin layer separating air inspired from the environment from blood in the capillaries. This blood-gas interface is so thin that gases such as oxygen and carbon dioxide are able to diffuse across it.

Air from the environment is brought into the alveolus by breathing-in (inspiration) while pulmonary circulation fills the capillaries with blood; the blood-gas interface is so thin that oxygen and carbon dioxide are able to cross it by passive diffusion (18) a process illustrated in Figure 2-3 (20).

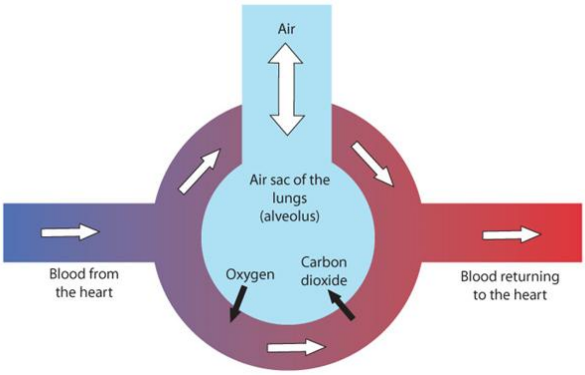

Figure 2-3: A simple model of gas exchange in an alveolus. Air fills up the alveolus and is separated from blood in the capillaries by the blood-gas interface. Carbon dioxide from the blood is diffused across the interface into the alveolus and eventually expired to the environment; oxygen from the air diffuses across the interface and is carried into the body by the blood.

2.3 MECHANICS OF BREATHING

Expansion and contraction of the chest tissue is accomplished by changing the volume of the chest cavity, this is done in two ways: it can be lengthened or shortened by movement of the diaphragm and its diameter can be increased by an elevation of the ribs. Normal resting breathing is done almost completely by contraction and relaxation of the diaphragm, when the muscle contracts it pulls the chest cavity outward, causing the lower tissue of the lungs to expand. When the diaphragm relaxes the *elastic recoil* of the lung tissue returns the lung to its previous size, making air flow out of the lungs (expiration). These volume changes cause changes in pressure within and around the lung, these pressure changes in turn are what cause flow of air in and out of the lungs (21).

At the beginning of inspiration pleural fluid is under a constant slight negative pressure of about -5 centimeters of water (cmH_2O) relative to atmospheric pressure (which convention sets at 0 cmH2O), holding the lung tissue against the chest wall but providing freedom of movement, as the chest cavity volume increases during inspiration *pleural pressure* changes to about -7.5 cmH_2O, expanding the lungs (21). However, it is alveolar pressure that causes airflow in and out of the lungs. Figure 2-4 (21) illustrates changes in lung volumes as related to alveolar and pleural pressures.

The *general gas law* shown in equation (2-1) states that at a constant temperature *(T)* an increase in volume *(V)* will lead to a decrease in pressure *(P)*, during inspiration inflation of the lungs caused by change in pleural pressure increases the diameter and volume of the alveoli therefore decreasing the pressure inside the alveoli to below that of atmospheric pressure making air rush into the lungs.

During expiration, pulmonary cavity volume decreases and elastic recoil of the lungs and alveoli forces them to shrink; this causes a pressure increase forcing expiration of air (18).

$$\frac{P_1 V_1}{T} = \frac{P_2 V_2}{T} \quad (2\text{-}1)$$

The body's airway passages have properties such as such as airway diameter, viscosity and elastic recoil; these properties act by opposing the movement of air in and out of the lungs that create respiratory impedance, a concept which is further examined in sections ahead.

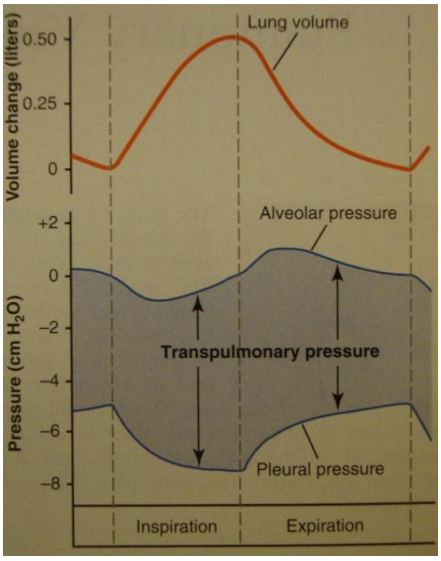

Figure 2-4: Changes in lung volume as related to changes in alveolar pressure and pleural pressure. Negative pressure within the alveoli forces air into the airways while positive pressure forces air out of them.

2.4 FORCED OSCILLATION TECHNIQUE AS A PULMONARY FUNCTION TEST

Spirometry measures lung volumes and airflow during specific breathing maneuvers such as maximum inspiration and rapid expiration as illustrated in Figure 2-5 (22), these measurements are then used to determine parameters of pulmonary function such as Forced Vital Capacity (FVC) and Forced Expired Volume in 1 Second (FEV_1). Spirometry provides good measures of airway obstruction, however, it provides no useful indices of small airway impairment (SAI) and in detecting diseases characterized by peripheral airway inflammation and impairment such as asthma and COPD, such an index could prove to be very useful (23). FOT has been shown to provide useful indices of SAI (24), furthermore, IOS reflects changes in airways in response to inhaled corticosteroids (ICS) (25)- (30).

Traditional testing methods such as spirometry measure pulmonary function during forced respiratory actions, in contrast, FOT requires little more than passive cooperation from the subject for the duration of the test.

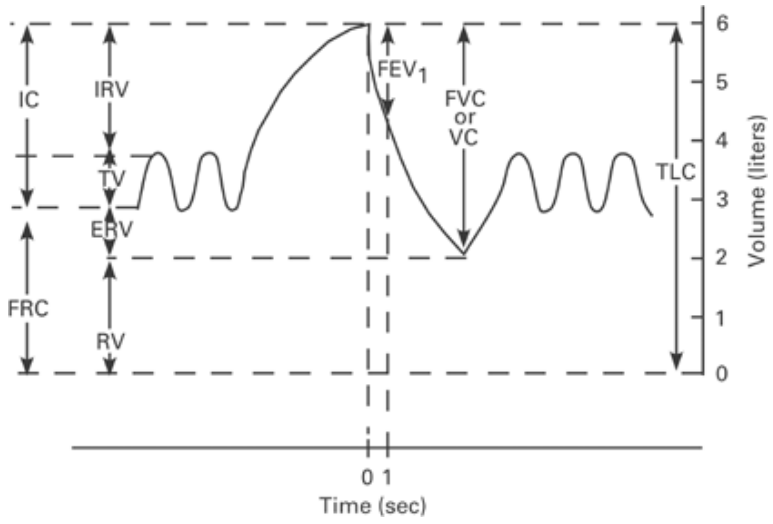

Figure 2-5: A spirogram, used to determine parameters of lung function such as Forced Vital Capacity (FVC), Total Lung Capacity (TLC) and Forced Expiratory Volume in 1 second (FEV_1), one of the most common indices used to determine respiratory abnormalities.

When using FOT a subject is artificially ventilated through the mouth, superimposing a synthetic airflow over normal breathing, at which point pressure and airflow measurements are obtained using transducers and then used to calculate the respiratory impedance characteristics of the airways, lungs and chest. DuBois' 1956 paper *"Oscillation Mechanics of Lungs and Chest in Man"* showed that respiratory function can be assessed by FOT, establishing methods used to obtain accurate, relevant and reproducible measurements of respiratory impedance (5).

2.4.1 FOT Excitation Signals

FOT has evolved since then and several excitation signals are now in use, each offering distinct advantages and disadvantages:

2.4.1.1 Random noise

This is a non-periodic signal containing a homogenous power distribution over a specified frequency range; it has the main advantage of being uncorrelated to normal breathing. However, it offers poor signal-to-noise ratio, creates leakage effects, and can be more complicated to work with than other signals, especially when modeling the resulting measurements require fractional-order models for proper results (31).

2.4.1.2 Sinusoids

Using sinusoids as an excitation signal provides high signal-to-noise ratio and provides unbiased estimations. However, when using a sine wave, only one frequency point is stimulated providing very limited information on the frequency response of the lungs. This creates the need for multiple sine waves, however, in order to keep the signal's power spectrum within linearity and comfort throughout the test the power of the signal is limited to peak-to-peak amplitude lower than 0.3 kPa (32).

2.4.1.3 Impulses

This type of signals uses a short, aperiodic pulse to stimulate the respiratory system. There are several advantages of using this type of signal including improved time-resolution when compared to random noise excitation signals. Because this type of signal used in IOS and this research a more in-depth review will be given in chapter 3.

2.4.2 Respiratory Impedance

In its simplest form gas flow (F, in liters per second), pressure (P, in cmH_2O) and resistance can be related by eq. (2-2) which tells us that resistance is the ratio of pressure change and airflow (18).

$$F = \Delta P / R \tag{2-2}$$

However, respiratory impedance is a force that affects the rate of airflow through the respiratory system in a non-uniform manner, for example, air near the center of the airway will flow differently than air closer to the airway wall. Because of this non-uniform change in airflow, respiratory impedance can be described as a complex quantity requiring both resistive (*resistance*) and reactive (*inertance* and *compliance*) components, describing both impedance magnitude and phase, respectively.

2.4.2.1 Resistance

If one were to think of a simple hollow tube with air flowing in at one end it's easy to imagine a force at that end opposing the movement of air into the tube. Similarly, one can think of *airway resistance* as a non-elastic friction force opposing respiration, which is created by the airways' own volume.

Since equation (2-2) tells us that pressure is directly affected by volume, increase in airway size during inspiration will decrease pressure and therefore resistance; during expiration, reduced airway size increases resistance. That same equation also tells us that at narrowest airways, such as bronchioles and alveoli resistance is high enough to make diffusion the main force driving airflow and most pressure change (or pressure *dissipation*) will occur due to resistance of the upper central airways (33), hereafter referred to as R_C (all resistances in kPa/(l/s)) [1]. This was confirmed by Macklem and Mead's direct pressure measurements: using catheters placed in 2mm distal or *peripheral* airways they determined that oscillatory pressures delivered to the trachea were 80% to 100% dissipated when they reached peripheral airways. They also noted that global peripheral resistance, which can be thought of as a network comprised of many resistances in a parallel arrangement, is very small except at very low lung volumes. From now on, his paper will refer to peripheral resistance as R_P (34).

---

1 Where 1 kilo Pascal (kPa) = 10.197 cmH_2O.

2.4.2.2 Inertance

In a pipe, the resistance created by the friction of its walls has a larger effect on air as it approaches the walls, in other words it disturbs air's velocity profile as illustrated in Figure 2-6 (14). However, the walls of airway passages in the body are covered with a viscous fluid. As frequency increases the force needed to move the fluid becomes more noticeable and further disturbs the velocity profile, creating more pressure at the walls (14). Higher pressure results in a larger viscous resistance thus creating an overall resistance with a positive frequency-dependant characteristic. This characteristic of the airways is called inertance and will be henceforth referred to in this paper as I (in kPa/(l/s^2)). Although inertance in the airways is usually very small and its clinical significance is so far ambiguous at best, it has been concluded that its effect is a very important characteristic of airway resistance (14).

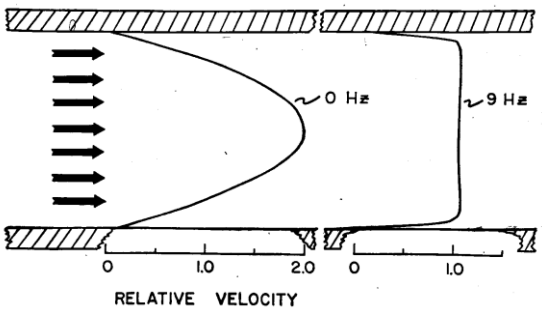

Figure 2-6: Illustration of velocity profiles of airflow in a pipe during steady flow and at about 9 Hz. The resistive friction force created by the viscous fluid on the airway walls changes with frequency, altering the velocity profile and ultimately creating a positive frequency-dependent airway impedance called inertance.

2.4.2.3 Compliance

As mentioned before, lung tissues possess elastic recoil, a property which describes how much a material opposes a stretching force. Its inverse property is compliance which describes a material's ability to stretch. In other words, high compliance means low elastic recoil, such a material is easily stretched but it takes a longer time to regain its original shape.

A simple pressure-volume curve can be used to determine total lung compliance, this method uses a *spirometer* to measure changes in lung volumes while simultaneously a pressure gauge measures change in pleural pressure. Compliance is then obtained by calculating the slope of the pressure-volume curve as shown in Figure 2-7.

Figure 2-7 also compares a normal pressure-volume curve to two abnormal curves, for example, if one obtains an abnormally high compliance it means that although the lungs are very elastic they also have low elastic recoil making expiration much more difficult, this is characteristic of the disease *emphysema*.

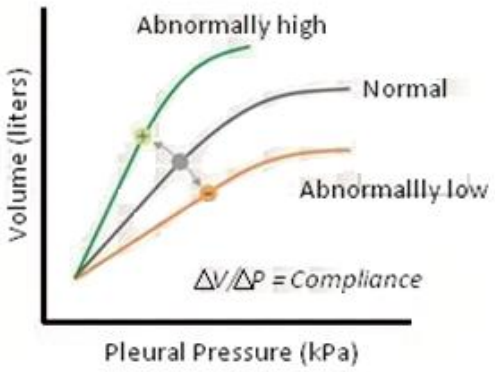

Figure 2-7: A pressure-volume curve can be used to determine compliance of the lungs by looking at the slope of the curve. An abnormally high compliance implies low elastic recoil and difficulties during expiration. An abnormally low compliance implies stiff tissues and diminished lung capacities.

2.5 RELEVANT PULMONARY DISEASES

Pulmonary disease is a very general term which includes many disorders such as asthma, chronic obstructive pulmonary disease, lung cancer, infections, influenza, pneumonia and many others. However, this study focuses on those conditions that are diagnosed using lung function tests such as spirometry and FOT; these conditions all affect the peripheral airways where gas exchange occurs and this study often refers to them as creating small airway impairment (SAI):

2.5.1 Chronic Obstructive Pulmonary Disease (COPD)

COPD is a condition that includes *emphysema* and *bronchitis*; it is also commonly a combination of the two. Emphysema is characterized by a loss of elastic recoil in the alveoli, making exhalation difficult. Bronchitis is inflammation (and therefore airway diameter reduction) of the bronchi usually accompanied by excess mucus in those airways.

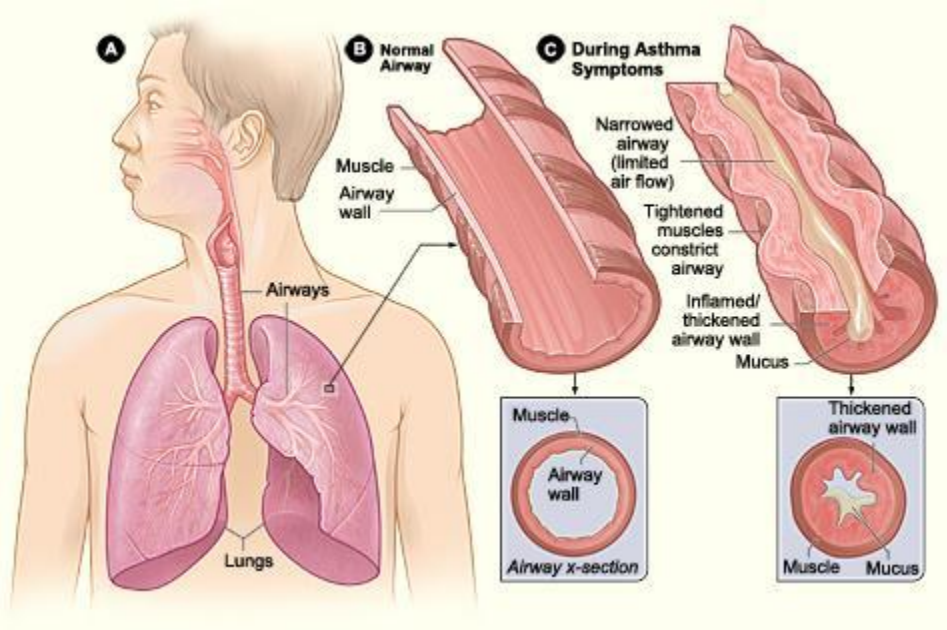

Figure 2-8: A comparison between normal airways and airways during an asthmatic episode during which airway diameter is greatly reduced, limiting air flow.

2.5.2 Asthma

Asthma is a respiratory disorder, which could be classified as COPD; the main difference being that unlike COPD, asthma is marked by acute exacerbations followed by symptom-free periods. It is characterized by airway inflammation accompanied by excess mucus production; the resulting airway narrowing reduces overall airflow and obstructs small airways. Figure 2-8 (35) illustrates the effect of an asthmatic episode on airways.

2.5.3 Fibrosis

Fibrosis is a restrictive lung disease, which is caused by damage, inflammation and scarring of the tissues surrounding the alveoli, as well as reduced lung compliance. It impairs the lung's ability to expand and therefore reduces total lung capacity.

Chapter 3: IMPULSE OSCILLOMETRY SYSTEM

Impulse Oscillometry System (IOS) is a commercially-available realization of FOT and a testing method used to determine a subject's level of pulmonary function by providing measurements of resistance and reactance of the respiratory system. Other methods such as spirometry, assess pulmonary function during forced breathing maneuvers therefore beyond lacking useful SAI indices as mentioned before, spirometry tends to be a difficult test to perform by subjects unable to follow directions such as small children and those that are unable to perform the necessary maneuvers such as the elderly or very ill.

In contrast, IOS requires minimal cooperation from the patient: mostly wearing nose clips and tightening the lips and cheek muscles to avoid air-leakage as it can adversely affect testing quality. Beyond that the subject must simply breathe normally, avoid as much movement as possible and bear a bit of discomfort from the very small bursts of air, which are superimposed on tidal breathing.

3.1 IMPULSE SIGNALS

As mentioned in chapter 2, there are several types of excitation signals used in FOT. For all variations of the technique retain the same basic idea which is to apply an external pressure signal and superimpose it on normal breathing. Using said pressure signal and the resultant air flow, mechanical impedance is then determined.

Among possible excitation signals that can be used is the impulse signal used by IOS and this study. One of the main advantages of impulse signals when compared to random noise is the possibility of applying several (usually 5) impulses per second. Each applied impulse provides an impedance measurement thus increasing the time resolution of the test (36).

A true Dirac-impulse is defined as having infinite magnitude for an infinitesimal duration; such an impulse contains all frequencies with their power distributed evenly across the entire frequency

spectrum. Real-world conditions do not allow for such signals to be generated and so the signals used in Impulse Oscillometry are not true Dirac-impulses and might be better described as "impulse-shaped signals" or pulses, the actual signal used in this technique has a rather small magnitude of around 0.3 kPa and lasts around 30-40 milliseconds (ms). The very-short pulse duration and its inherent sinusoidal-components allows for a relatively constant power spectra along the lower respiratory frequencies, which can be seen in fig Figure 3-1 (36).

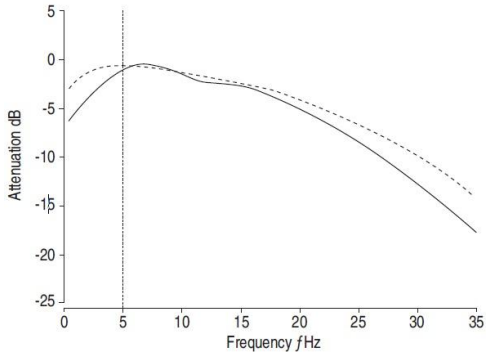

Figure 3-1: Power spectra of the impulse-shaped pressure signal used in IOS (dashed line) and the resulting flow (continuous line) plotted from 0.1 to 35 Hz. This study focuses on the 5 to 25 Hz range in which the power spectra is relatively constant and is less disturbed by respiratory harmonics.

This study uses data obtained for the 5 to 25 Hz frequency range; it can be seen in figure Figure 3-1 that frequencies below 5 Hz are more attenuated and therefore more affected by the higher harmonics of natural respiration (37) while higher oscillation frequencies are increasingly affected by "shunt" properties of the upper airways (36) and are therefore unreliable.

One important attribute of the pulse excitation signals used in IOS is their aperiodic nature. A characteristic of aperiodic signals is the resulting continuous spectra when transformed from time-domain to frequency-domain using Fast Fourier Transform (FFT). In contrast, other signals result in discontinuous (or discrete) impedance measurements containing only data points corresponding to the frequencies of its embedded sine components. Thus, many times when using signals other than impulses,

post-processing is necessary in order to smooth the resulting spectra; post-processing inherently diminishes the information contained in the spectra, this can be of particular importance in abnormal subjects whose results usually deviates from the normally smooth spectra (36).

3.2 IMPULSE OSCILLOMETRY SYSTEM

Flow and pressure measurements take place in the system's measuring-head shown in Figure 3-2 (36). Flow is measured by a heated pneumotachograph with a resistance of 36 $Pa*s*L^{-1}$ that provides a common-mode rejection ratio above 60 dB up to 50 Hz. Pressure is measured using a pressure transducer which is matched to the flow transducer in order to avoid measuring discrepancies due to technical differences between them. Pressure and flow signals are then sampled at 200 Hz and digitized with a 12-bit analog to digital converter (36).

The loudspeaker creates a volume displacement in 30-40 ms, this displacement in combination with the terminal resistor creates pressure signals in alternating directions with peak-to-peak amplitudes of about 0.3 kPa.

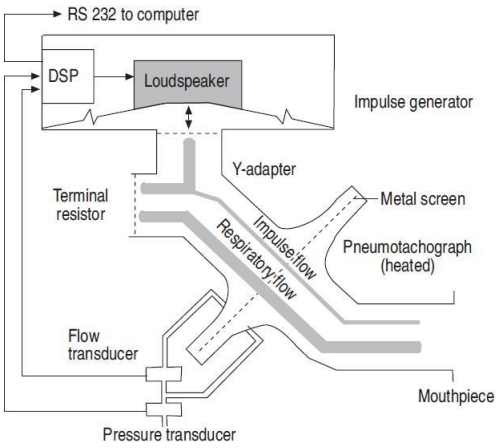

Figure 3-2: Diagram of the Impulse Oscillometry System measuring-head and components. The speaker generates pulse flows, which are represented by the shaded, slightly-thick line. Part of said flows exits through the terminal resistor ($0.1\ kPa*s*L^{-1}$) and the rest flows through the pneumotachograph and exits through the mouthpiece. Normal respiratory flow is represented by the thicker shaded line and exits through the terminal resistor.

3.3 RESPIRATORY IMPEDANCE AS MEASURED BY IOS

Respiratory impedance is defined as the Fourier transform of the ratio of pressure (*P*) and flow (*F*) of the superimposed oscillation after underlying respiration is removed (see eq. (3-1)). The resulting impedance spectrum is "complex" by nature, containing both magnitude and phase information.

(3-1) $Z(\omega) \equiv F\{z(t) = P(t)/F(t)\}$, where $F\{\ \}$ = "the Fourier transform of."

Impedance calculations are focused on individual impulses with the sampling duration proportional to the pulse rate, encompassing both the pressure and flow signals along with the respiratory system's reaction to them. Underlying respiration is removed by linearly approximating the baseline. Figure 3-3 (36) illustrates pressure and flow waveforms after underlying respiration has been removed.

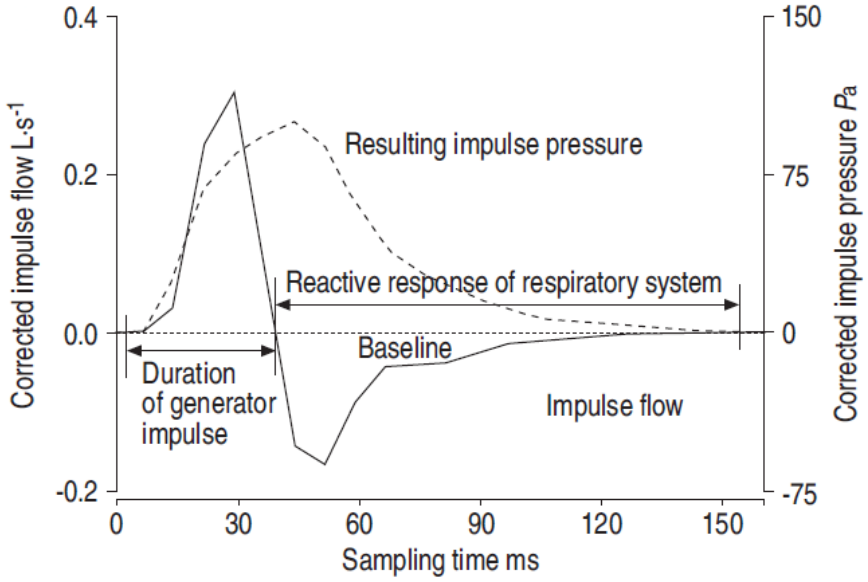

Figure 3-3: Traces of flow (continuous line) and pressure (dashed line) after underlying respiration is removed by baseline approximation. The sample includes the impulse generated by the loudspeaker, the resulting pressure signal and the respiratory systems reaction to the stimulus.

3.3.1 Complex Impedance

Corrected flow and pressure measurements are then used to calculate impedance as was described above; the resulting impedance is a complex quantity containing magnitude and phase information. A complex quantity is most commonly referred to as having both "real" and "imaginary" components, however, this study usually refers to those quantities as resistive (R) and reactive (X), respectively. Respiratory impedance is of the form shown in eq. (3-2) and Figure 3-4 illustrates sample spectra for both resistance and reactance.

(3-2) $Z(f) = R(f) + jX(f)$, where f = frequency and $j = (-1)^{1/2}$

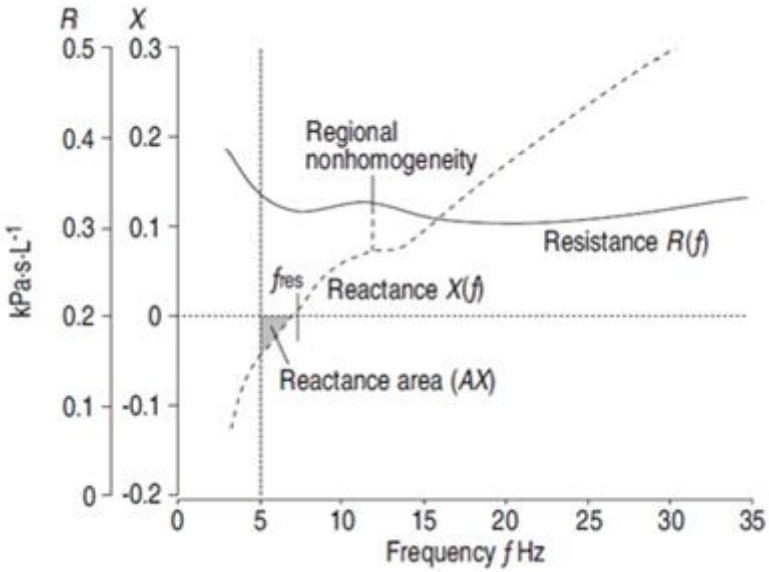

Figure 3-4: Respiratory impedance spectra as obtained by IOS testing, the continuous line represents respiratory resistance (R) and the dashed line represents respiratory reactance (X). The point at which reactance is exactly zero is called resonant frequency (*fres*) and at this point elastic and inertive properties of the respiratory system are in balance. Integrating the area under the reactance curve from 5 Hz to *fres* yields reactance area (AX), also known as the "Goldman Triangle", which has been proven to be a very important IOS diagnostic parameter.

3.3.2 Resistance

Respiratory resistance is created by the central and peripheral airways, lung tissue and chest wall. However, lung tissue and chest wall resistance are usually negligible and most of the measured resistance is dominated by the upper central resistance (34). Normal, healthy subjects possess airway resistance that is mostly independent from frequency with the exception of higher frequencies, which are affected by the upper airways "shunt" effect. This independence from frequency does not seem to apply to abnormal patients and is used as a measure of airway "normality".

3.3.3 Frequency-dependence of Resistance (fdR)

Airway obstruction, either central or peripheral, elevates respiratory resistance. However, central airway obstruction increases resistance evenly while peripheral airway obstruction creates a resistance measurement that is highest at lower frequencies and decreases as frequency increases. This negative frequency-dependent behavior is referred to as *frequency-dependence of R (fdR)*. Some have attributed *fdR* to upper airways "shunt" effect, however efforts made to remove *fdR* by applying oscillations to the entire head and upper neck and by pressing firmly on the cheeks have been unsuccessful (38)-(40). Intrapulmonary gas flow redistribution due to system nonhomogenities or changes in elasticity of peripheral airways has been used to explain *fdR* (36), furthermore, recent studies have shown a close correlation between *fdR* and other indices of peripheral airway function (41).

3.3.4 Reactance

Respiratory reactance is created by the inertive properties of the airways and elastic characteristics of the airways and tissues. These properties, referred to respectively as Inertance (*I*) and Compliance (*C*) can be represented by eqn. (3-3):

(3-3) $X(f) = \omega I - 1/(\omega C)$, where $\omega = 2*\pi*f$.

Compliance as it relates to reactive impedance is by convention negative in sign and therefore, not entirely the same as compliance in other contexts. Inertance, on the other hand, is always a positive frequency-dependant quantity and while compliance dominates lower frequencies, inertance is more predominant at higher frequencies.

3.3.5 Resonant Frequency

Resonant frequency (*fres*) is defined as the point in the frequency spectrum at which reactive inertance and compliance are equal and the overall reactance is exactly zero:

(3-4) $\omega_0 I = 1/(\omega_0 C),$ where $\omega_0 = 2*\pi*fres$.

Although "normal" *fres* can be said to lie somewhere between 7 to 12 Hz, the number by itself is useful mostly as a guide in separating low-frequency from high-frequency reactance. Resonant frequency tends to vary widely and usually decreases with age, and diseases both obstructive and restrictive tend to increase *fres* (36).

3.3.6 Reactance Area (AX or Goldman Triangle)

Low-frequency *X(f)* is dominated by compliance and therefore expresses the respiratory system's ability to store capacitive energy, especially in the peripheral region. This ability can be reduced due both to hyperinflation or stiffness of the lungs and is reflected as increasingly negative values in the lower frequency reactive spectrum at 5 Hz (*X(5)*); *X(5)* by itself is thus unable to distinguish the type of abnormality in the lung, however, said distinction can be made using other information and is usually non-problematic in clinical settings (36).

Low-frequency reactive impedance is said to lie below *fres*, and in order to take advantage of the continuous reactive frequency spectrum (and in a sense, its shape) an index designated as reactance area

was created (*AX*). This index can be seen in Figure 3-4 as the area created by the reactive spectrum below *fres* and the frequency axis; it can also be defined by equation 0 (36).

$$AX = \int_{5}^{fres} X(f)df. \quad (3\text{-}5)$$

As mentioned before, low-frequency reactance reflects peripheral airway function, *AX* (Goldman Triangle) is a quantity that reflects this whole region, and serves as an index of peripheral airway obstruction, correlates closely with *fdR* (42) and, as will be later discussed in detail, also correlates very closely with model-derived parameters of peripheral compliance, tracks SAI, and can measure treatment effectiveness (29), (30).

Chapter 4: RESPIRATORY IMPEDANCE MODELING

In 1956 Arthur DuBois published his landmark paper entitled *"Oscillation Mechanics of Lungs and Chest in Man"* (5). In it he describes the premise, methodology and results of his FOT experiments. DuBois proposes that much information can be gained by analyzing the frequency response of a subject's respiratory system, such as its respiratory compliance, inertance and resistance. For this purpose he employed a pump to generate transthoracic pressures, which he applies at the mouth, and used a capacitance manometer to measure said pressures. The pump strokes were sinusoidal and because all periodic motions can be broken down into sinusoidal components, DuBois argued that using sinusoidal pressures at several frequencies will provide the benefits of other types of motion (such as random noise or impulses). Furthermore, sinusoids are easy to analyze mathematically, which was especially important at the time.

The respiratory system is intricate, branching many times into distinct compartments each of them with unique characteristics. Its mechanical properties, resistance, inertance and compliance, are not evenly distributed throughout the whole system and DuBois recognized that the behavior of a subject's total frequency response is the sum of several distinct reactions that the system has to an applied external pressure. As such, DuBois presented a mechano-acoustical model made-up of several elements meant to represent distinct areas of the respiratory system. However, perhaps because characterizing frequency response of a system is an integral part of electrical engineering as a discipline, he also included the analogous relationship presented here in Table 4-1 (5).

Table 4-1 states that for analytical purposes, a mechanical flow, such as air, is equivalent to an electrical current applied to a circuit (current flow) and the resulting air pressure is equivalent to electrical potential. This relationship is extended to the components of a mechanical system and those present in an electrical one: Mechanical resistance is equivalent to electrical resistance in the sense that they are both purely resistive, they have no phase effect on the applied external signal. This comparison holds true for

the remaining model elements, mechanical capacitance and mechanical compliance both create a lag on air pressure with respect to air flow; similar to electrical capacitance, which makes electric potential lag electric current. Finally, mechanical inertance creates a lag in air flow with respect to air pressure whereas electrical inductance creates a lag in electrical current with respect to electrical potential.

Table 4-1: Analogous relationships between mechanical and electrical impedance.

MECHANO-ACOUSTICAL	ELECTRICAL
Air flow	*Electric Current*
Air pressure	*Electric Potential*
Resistance	*Resistance*
Capacitance	*Capacitance*
Compliance	*Capacitance*
Inertance	*Inductance*

Because of several factors, most prominent of them being technological advances, FOT has evolved much since its origins. However, the use of electronic circuits as respiratory impedance models remains commonplace and mechanical models are rarely used in FOT studies.

4.1 RIC MODEL

As mentioned in section 3.3 the different properties of the respiratory system that affect respiratory impedance are resistance, inertance and compliance; these properties create a complex impedance containing both resistive (real, *R(f)*) and reactive (imaginary, *X(f)*) components. This relationship can be summarized by equation (4-1):

$$Z(f) = R(f) + jX(f), \qquad \text{where } j = (-1)^{1/2}. \tag{4-1}$$

Now, if one considers reactance in its simplest form (eq. (3-3)) then, by substituting into eq. (4-1), for a single point in the frequency spectrum impedance can be considered to be:

(4-2) $Z = R + j[\,\omega I - 1/(\omega C)]$, where $j = (-1)^{1/2}$ and $\omega = 2*\pi*f$.

Equation (4-2) is effectively the *RIC* (Resistance-Inertance-Compliance) model; its circuit diagram is pictured in figure Figure 4-1 (10).

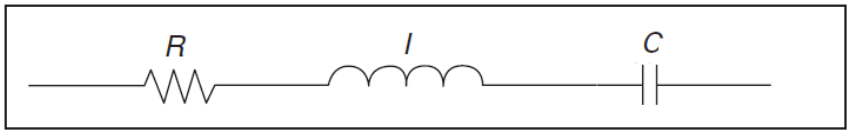

Figure 4-1: The RIC respiratory impedance model contains a single element each for airway resistance *(R)*, inertance *(I)* and compliance *(C)* respectively.

This model considers resistive impedance as completely frequency-independent and reactive impedance as completely frequency-dependent; in other words, this model uses its *R*-parameter to estimate resistive impedance only (Z_R) while the *I*-*C* network simulates reactive impedance only (Z_X). Because of this, the model is easy to use and understand. On the other hand, due to the lack of "local" parameters such as one assigned specifically to simulate alveoli compliance, it doesn't provide with much useful information beyond what can be obtained using other pulmonary function tests such as spirometry. Furthermore, because the model fails to take into account frequency-dependence of *R* oftentimes present in subjects with respiratory abnormalities (see figure Figure 4-2), it does a poor job modeling subjects presenting high *fdR* which can lead to elevated estimation errors (10).

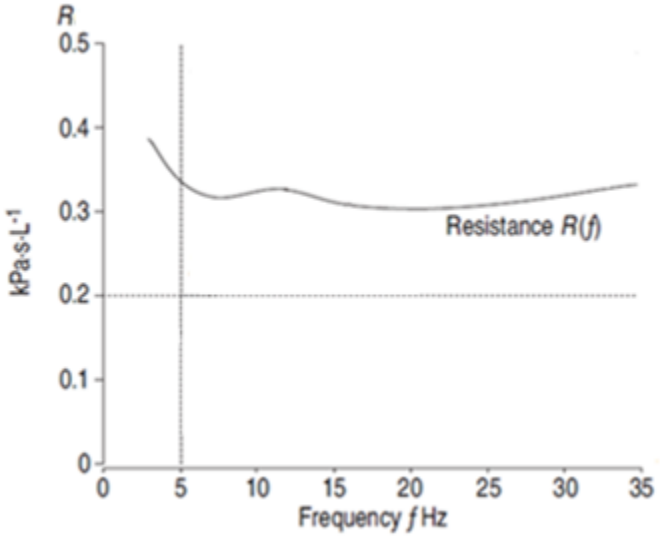

Figure 4-2: A sample IOS measurement showing resistance *R(f)*. This particular subject shows an obvious frequency-dependence of resistance, a phenomenon which the RIC model fails to accurately estimate.

4.2 DUBOIS' MODEL

Besides the previously mentioned contributions and his mechano-acoustical model, in his paper DuBois also introduced a respiratory impedance model based on electric circuits, the model diagram is shown in figure Figure 4-3 (5), (10).

DuBois' model, in contrast to the RIC model, is meant to be more physiologically significant. By "compartmentalizing", this model seeks to provide estimates for mechanical properties in distinct regions: tissues (R_t, I_t and C_t), airways (R_{aw} and I_{aw}) and alveoli (C_g). This model's impedance equation is much more complicated than the RIC equation as shown in eq. (4-3). Not considering circuit arrangement, due to the complex nature of electric capacitance and inductance, each element added to a circuit will usually greatly increase its resulting impedance equation.

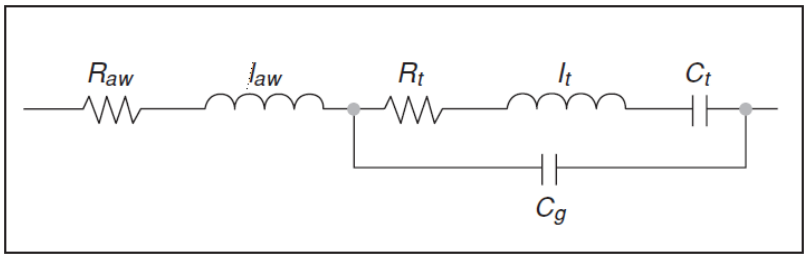

Figure 4-3: DuBois' respiratory impedance model contains elements representing airway and tissue resistance (R_{aw} and R_t), airway and tissue inertance (I_{aw} and I_t) as well as tissue and alveolar compliance (C_t and C_g).

$$(4\text{-}3) \quad Z = R_{aw} + j\omega I_{aw} + \frac{\omega^2 R_t {C_t}^2}{\omega^6 (C_g C_t I_t)^3 + \omega^4 \left[C_g C_t \left(C_g C_t {R_t}^2 - 2I_t (C_g + C_t)\right)\right] + \omega^2 (C_g + C_t)^2} -$$

$$\frac{j\omega[\omega^4 C_g {C_t}^2 {I_t}^2 - \omega^2 C_t (2C_g I_t + C_t I_t - C_g C_t {R_t}^2) + (C_g + C_t)]}{\omega^6 (C_g C_t I_t)^3 + \omega^4 \left[C_g C_t \left(C_g C_t {R_t}^2 - 2I_t (C_g + C_t)\right)\right] + \omega^2 (C_g + C_t)^2}$$

Although this model is more physiologically realistic than the RIC model it does have several important disadvantages: its mean estimation error for reactance data is somewhat large and it's not uncommon to obtain values of C_g that are too great for them to be physiologically possible (10).

4.3 MEAD'S MODEL

Perhaps the most physiologically accurate of the models presented in this study, Mead's respiratory impedance model seeks to simulate distinct mechanics for the chest wall and lung tissue (C_w and C_l) as well as central resistance and inertance (R_c and I), peripheral resistance and compliance (R_p and C_p) and extrathoracic "shunt" compliance (C_e) (4), an illustration of this electric respiratory impedance model can be seen in figure Figure 4-4.

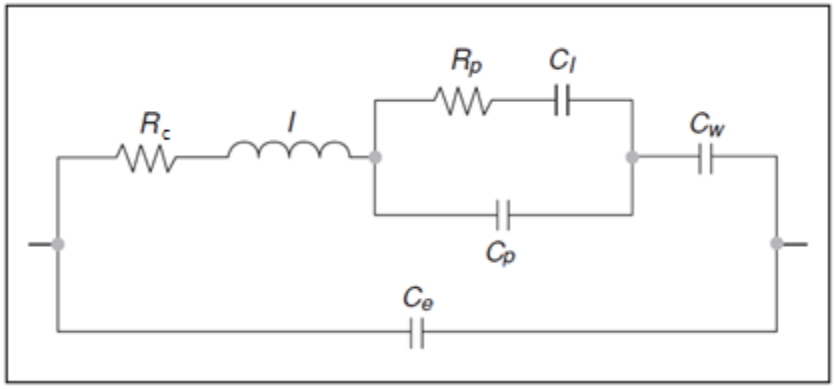

Figure 4-4: Mead's respiratory impedance model contains parameters representing chest wall and lung tissue compliance (C_w and C_l), central resistance and inertance (R_c and I), peripheral resistance and compliance (R_p and C_p) and extrathoracic "shunt" compliance (C_e).

The use of seven parameters in Mead's model results in a complicated impedance equation (4):

(4-4) $$Z = \frac{-j}{\omega C_e} || Z_m$$

Where:

(4-5) $$Z_m = \frac{R_p {C_l}^2}{\omega^2 {R_p}^2 {C_p}^2 {C_l}^2 + (C_p + C_l)^2} + R_c + j\left(-\frac{\omega^2 {R_p}^2 {C_p}^2 {C_l}^2 + C_p + C_l}{\omega\left[\omega^2 {R_p}^2 {C_p}^2 {C_l}^2 + (C_p + C_l)^2\right]} + I - \frac{1}{\omega C_w}\right) = R_m + jX_m$$

And so:

(4-6) $$Z_R = Re(Z) = \frac{R_m}{1 - 2\omega C_e X_m + \omega^2 {C_e}^2 ({R_m}^2 + {X_m}^2)}$$

(4-7) $$Z_X = Im(Z) = \frac{X_m - \omega C_e ({R_m}^2 + {X_m}^2)}{1 - 2\omega C_e X_m + \omega^2 {C_e}^2 ({R_m}^2 + {X_m}^2)}$$

Mead's model provides for very good data fit, however, when using IOS data it presents two important problems: the parameter estimates for lung tissue compliance and chest wall compliance very often result in extremely large values, too large to be realistic; this problem coupled with the fact that

these parameters hold no significant diagnostic value make the model overcomplicated for IOS data (10), (43), (44). These issues, which this study sometimes refers to as model "blow-ups" will be explored in depth in Chapter 7:.

4.4 EXTENDED-RIC (eRIC) MODEL

This model shown in figure Figure 4-5 (10) is intended to be a simplification of Mead's model which is achieved by removing parameters for lung tissue compliance (C_l), chest wall compliance (C_w) and extrathoracic "shunt" compliance (C_e). The reasoning behind such a simplification is that their lack of diagnostic significance and tendency towards unrealistic values make those parameters undesirable. Although undesirable and unnecessary are not one in the same, this study seeks to prove in further chapters that this is in fact the case when using IOS data.

In spite of its relative simplicity the eRIC model provides for good data fit, comparable in mean total error to DuBois' model but with better reactive data fit (10). Estimation errors are also in the same range as Mead's model and as will be explored in further chapters, out of all the models presented here, it provides the best correlations between estimated parameters and diagnostically significant IOS indices such as *AX* and *fdR* (41).

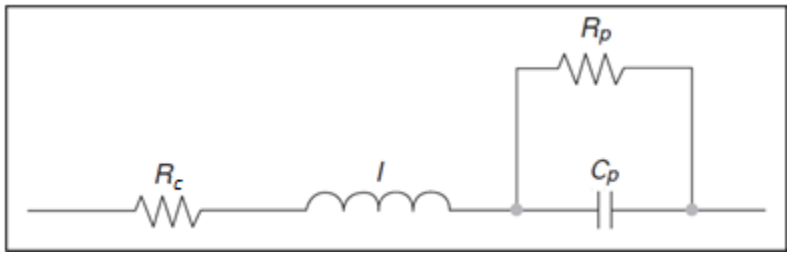

Figure 4-5: The extended-RIC model can be considered a simplification of Mead's model. This model has four parameters representing central resistance (R_c), inertance (I), peripheral resistance (R_p) and peripheral compliance (C_p).

The *eRIC* model has the following impedance equation:

$$(4\text{-}8) \quad Z = R + \frac{R_p}{1+(\omega R_p C_p)^2} + j(\omega I - \frac{\omega {R_p}^2 C_p}{1+(\omega R_p C_p)^2})$$

And so:

$$(4\text{-}9) \quad Z_R = R + \frac{R_P}{1+(\omega R_P C_P)^2}$$

$$(4\text{-}10) \quad Z_X = \omega I - \frac{\omega {R_P}^2 C_P}{1+(\omega R_P C_P)^2}$$

4.5 AUGMENTED-RIC (aRIC) MODEL

The augmented-RIC model shown in figure Figure 4-6 can also be thought of as a simplification of Mead's model, although it was originally introduced as an alternative to eRIC to better model IOS data (45).

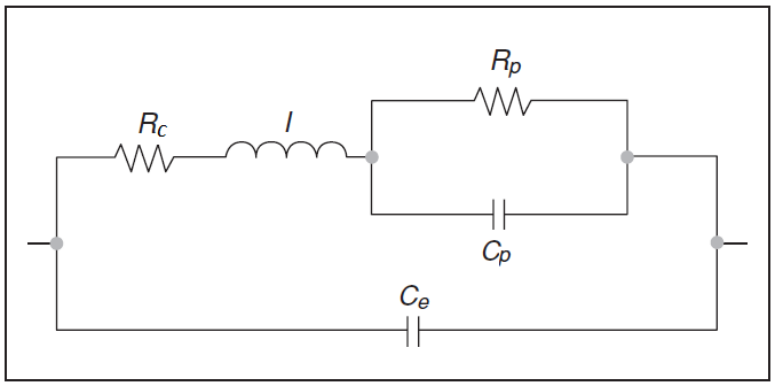

Figure 4-6: The augmented-RIC can also be considered a simplification of Mead's model. It has parameters for central resistance (R_c), inertance (I), peripheral resistance (R_p), peripheral compliance (C_p) and extrathoracic compliance (C_e).

This model's impedance equation is:

(4-11) $$Z = \frac{A(RA+R_p)}{[A(1-\omega^2 IC_e)+(\omega^2 {R_p}^2 C_p C_e)]^2+[\omega C_e(RA+R_p)]^2} + j\frac{\omega(IA-{R_p}^2 C_p)[A-\omega^2 C_e(IA-{R_p}^2 C_p)]-\omega C_e(RA+R_p)^2}{[A(1-\omega^2 IC_e)+(\omega^2 {R_p}^2 C_p C_e)]^2+[\omega C_e(RA+R_p)]^2}$$

Where:

(4-12) $$A = 1 + (\omega R_p C_p)^2$$

And so:

(4-13) $$Z_R = \frac{A(RA+R_p)}{[A(1-\omega^2 IC_e)+(\omega^2 {R_p}^2 C_p C_e)]^2+[\omega C_e(RA+R_p)]^2}$$

(4-14) $$Z_X = \frac{\omega(IA-{R_p}^2 C_p)[A-\omega^2 C_e(IA-{R_p}^2 C_p)]-\omega C_e(RA+R_p)^2}{[A(1-\omega^2 IC_e)+(\omega^2 {R_p}^2 C_p C_e)]^2+[\omega C_e(RA+R_p)]^2}$$

During the time of this model's conception data that included frequencies up to 35 Hz was still commonly used. Higher frequency measurements tend to increase in the respiratory system resistance (R) and the eRIC model is unable to simulate the positive frequency-dependence. It has since been shown that higher frequencies are unreliable due to the "shunt" effect of upper airways. Also worth noting is that eRIC and aRIC parameter estimates are very similar, however, aRIC does provide consistently smaller estimation errors than eRIC. Both of these models will be extensively explored in the following chapters and therefore the present section doesn't include important information which is better suited for later sections.

4.6 A BRIEF NOTE REGARDING OTHER MODELING EFFORTS

Technological advances in FOT, both in equipment and computational capabilities, have led to an increased versatility when researching this pulmonary function test. Much research has since focused on using much wider frequency ranges (46), (31), (15), others focus on increased model complexity striving

for better data fit (13), (14), (16) or in most cases both. However, since this study focuses on those human respiratory system impedance models proven as best suited for modeling IOS data obtained for relatively low frequencies, the more complex models developed for higher frequency excitation will not be of interest here.

Chapter 5: MODEL PARAMETER ESTIMATION

Asthma and similar lung diseases are a very important health concerns that at the very least diminishes a patient's quality of life and sometimes can even prove fatal; yet spirometry, the most common of pulmonary function tests is not a reliable diagnostic method: In children it fails to detect diminished pulmonary function unless it's particularly aggravated (3) and it lacks a useful index of small airway impairment (SAI) (23). On the other hand, IOS has been proven to provide such indices (with *AX* and *fdR*) (3), (24)- (30). Moreover, in some cases model-derived parameters have been shown to be even more sensitive than *fdR* in tracking lung function and distinguishing health and disease (28).

Therein lays the importance of respiratory impedance modeling. In the practical aspect, it simplifies IOS testing by providing more intuitive results: For specific properties, in specific lung regions, it provides a numerical value that makes physiological sense; as opposed to complex impedance waveforms and complicated IOS indices. More importantly, model parameters may prove to be very useful, be it by themselves or in conjunction with well-established IOS parameters. Concluding that there exists a need for model-derived parameters leads to the matter of calculating said parameters, which is the topic of this chapter.

5.1 MODEL PARAMETER ESTIMATION AS A NONLINEAR LEAST SQUARES ERROR MINIMIZATION PROBLEM

Parameter estimation in essence is determining the best combination of values for model parameters which minimize the difference between IOS impedance data at discrete frequencies and the impedance produced by the model using the determined parameter values. This process or parameter estimation, also known as regression, can be approached with several techniques the most common of which is the least squares (LS) approach. It is not only the most common error criterion but it's also accurate, computationally efficient and readily available in software packages such as *Matlab*.

For any given respiratory impedance model its impedance is represented by Z. We then set a residual function *r* such that:

(5-1) $r_i(\boldsymbol{p}) = Z_i - (R_i + jX_i)$, where $i = 5, 10, \ldots, 25$, the discrete frequency points, $\boldsymbol{p}$ is the vector of model parameters and $R_i + jX_i$ are the impedance values as measured by IOS.

Then estimating model parameters becomes a LS minimization problem, where *E* is the sum of squared residuals:

(5-2) $min\,[E = \sum_5^{25} r_i(\boldsymbol{p})^2]$

Whether the LS minimization problem is linear or nonlinear depends on the model used. In the case of simpler models such as *RIC* linear regression can be used, however, this study focuses on the *aRIC* and *eRIC* models which are nonlinear systems and therefore the problem itself becomes nonlinear. Solving this type of problem is a very involved and complicated process. Fortunately this area of study is very well researched and many methods for solving such problems exist, the most common and efficient of which can be implemented using *Matlab*'s *lsqnonlin* function.

5.2 AVOIDING LOCAL MINIMA

Solving this type of problem is a difficult task there is the possibility that multiple solutions (or rather, multiple minima) exist and in the presence of multiple minima it is not uncommon for a nonlinear method to find local minima. A local minima can be thought of as a "solution' to the minimization problem because it will fit the minimization method's solution criteria, what this study refers to as a stopping criteria. However, local minima by definition are not the best solutions and must be avoided. An illustration of the local minima phenomenon is shown in figure Figure 5-1.

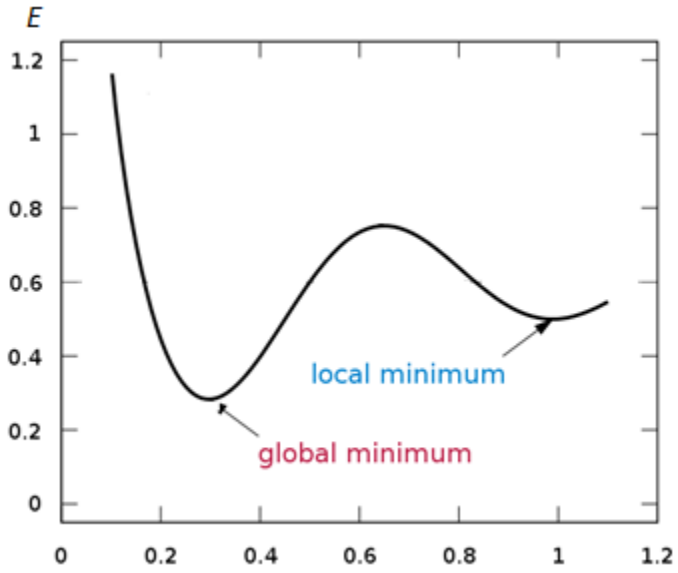

Figure 5-1: A simple illustration of global and local minima for an arbitrary error function *E*. Because nonlinear least squares estimation algorithms are descent-based the possibility of finding local minima is ever-present and therefore, care must be taken in choosing appropriate initial conditions for the minimization problem.

To avoid this problem an algorithm was written that uses a uniformly distributed pseudorandom number generator to set arbitrary initial estimation values or "guesses". Essentially, the algorithm runs a certain amount of user-defined trials of the *lsqnonlin* function, each time making sure the current initial points have not yet been tried. The result of each trial is saved and compared to each other; the algorithm then returns the parameters found that best solves the minimization problem, i.e. the set of parameter values that yields the smallest estimation error.

5.3 THE NEED FOR CERTAIN NUMERICAL CONSTRAINTS

Imposing a numerical constraint on an optimization algorithm forces that algorithm to find a solution that minimizes the estimation error while only using those numbers that satisfy the constraint. In the case or respiratory impedance models the obvious numerical constraint is that since negative resistance, compliance or inductance are not realistic, it has to be imposed on the estimation routine that no result should be of negative value. The lower bound then, for all model parameters, is zero.

Another consideration has to be made for those models such as Mead's whose parameters C_l and C_w have shown a tendency to result in estimations that are too large, sometimes by several orders of magnitude (10), (43), (44). In those cases one might work under the assumption that physiologically-unrealistic parameter estimations must not be real solutions, or at the very least they are not useful solutions and therefore upper bounds are set. The value of the upper bound depends on the parameter being estimated, for inertance an unrealistic value might be 0.1 kPa/(l/s^2) (5), whereas for lung tissue compliance it's probably closer to 1.5 l/kPa (47).

Because this study focuses on the *aRIC* and *eRIC* models, constraints other than lower bounds were very rarely used and mostly only when working with Mead's model. When using Mead's model C_l and C_w had equal upper boundaries depending on the subject's height: If height was <140 cm an upper boundary of 1.5 l/kPa was used, when the subject's height was 140 cm or more the upper boundary was set to 2 l/kPa. In the very rare cases were Mead's model was used and no height information was available the upper boundary was then set to 2 l/kPa.

5.4 STOPPING CRITERION

A stopping criteria is a condition that when reached causes the algorithm to stop and return a solution to the user. The most commonly imposed stopping condition is shown in eq. (5-3), in which ϵ is a real number, ideally very close to zero. This stopping condition compares the estimation error to ϵ, if the error is less than ϵ the algorithm stops and the parameter values (vector $\boldsymbol{x}$) are returned as they are considered a satisfactory solution. If the condition is not met, the algorithm will keep going until a satisfactory solution has been found or another stopping condition has been reached.

(5-3) $$[E = \sum_5^{25} r_i(\boldsymbol{p})^2] < \epsilon$$

Because mean estimation errors vary widely depending on the model being used this particular criteria is not used and instead two others were implemented.

5.4.1 Step Size

This stopping condition works under the assumption that if the estimation algorithm keeps converging on the same parameter values, then the algorithm has found a minimum (either local or global). For a real number ϵ_S the algorithm will stop if the following condition is met:

(5-4) $$max[abs(\boldsymbol{x} - \boldsymbol{x'})] < \epsilon_s$$

Where $\boldsymbol{x}$ is a vector containing the current iteration's estimated parameter values and $\boldsymbol{x'}$ contains the previous iteration's estimated parameter values. In other words, the algorithm first determines the amount of change for each parameter from an iteration to the next, it then selects the largest of those changes and compares it to ϵ_s. If the stopping condition is met then the results are very similar and it is assumed a global solution has been reached. If the condition is not met, that is if the amount of change is too large, then the algorithm assumes that it has not yet reached a global minimum and continues until a stopping criteria is reached.

For this study ϵ_s was set to 0.5 X 10^{-5}. To provide better results and consistency throughout this study, a solution which meets this condition will not stop the algorithm entirely, but rather it considers the solution satisfactory for the current trial and stores it for later comparison to results from other trials. This is done to ensure that every dataset is put through the same number of trials and therefore the same number of distinct initial conditions.

5.4.2 Trials

A trial, in this particular algorithm, refers to the number of times the estimation algorithm is run, with different starting conditions each time. During each trial the optimization routine will run until a

minimum has been found, or until a large number of attempts (1000) to do so have been made. At the end of each trial the estimated parameter values are saved and the algorithm moves on to the next trial. After all trials have been completed the best result, i.e. the parameter values yielding the smallest estimation error, is returned to the user.

The purpose of multiple trials is to avoid local minima. By ensuring that each trial starts with different initial conditions the probability of stumbling upon local minima is greatly reduced. Estimations using a variety of datasets were observed to determine what an appropriate number of trials would be. It was observed that 10 trials were very often more than sufficient, very rarely would the best solution be found in later trials. However, this study uses 25 trials for calculating parameters for each data set.

5.5 MODEL PARAMETER ESTIMATION ALGORITHM

In this section a brief description of the algorithm used to determine model parameter values is presented. The algorithm itself was written and implemented in Matlab environment. For improved clarity and easier reading the working code is not presented in this work, instead, pseudo-code is used here. Since an algorithm is basically a procedure used to solve a certain problem, that procedure can be presented using high-level and somewhat informal language. This allows the reader to understand the procedure without requiring expertise in specific programming languages or techniques.

5.5.1 Pseudo-code

1. Initialize a variable p_r and set it to a very large but arbitrary number. Also, initialize a vector $\boldsymbol{p}$ with a number of elements equal to the number of parameters in the model being used.
2. For a user-defined amount of trials (as discussed in section 5.4.2), do the following during each trial:
   i. Initialize a uniformly distributed pseudorandom number generator to a unique state based on the system clock.

ii. Make an initial guess: Using the uniformly distributed pseudorandom number generator, create a vector containing a number of random elements equal to the number of parameters in the current model used.

iii. Run the nonlinear LS optimization function using the initial guess and predetermined numeric constraints. Store the estimated parameter values into a vector $\boldsymbol{x'}$ and the residual (or estimation error) into a variable r'.

iv. While the step size is smaller than ϵ_s or for at most one thousand iterations (as described in section 5.4.1), do the following:

   a. Run the nonlinear LS optimization function using the values stored in $\boldsymbol{x'}$ and the predetermined numerical constraints. Store the newly estimated parameter values into a vector $\boldsymbol{x}$ and the resulting residual into variable r.

   b. Determine the step size as described in eq. (5-4).

   c. Do the following:

      If $r < r'$. Set $\boldsymbol{x'} = \boldsymbol{x}$ and $r' = r$. Return to step iv.

      Otherwise, return to step iv.

v. Do the following:

   a. If $r' < p_r$. Set $\boldsymbol{p} = \boldsymbol{x'}$ and $p_r = r'$.

   b. Otherwise, continue to step 3.

3. Return vector $\boldsymbol{p}$ which now contains the parameter values that best fit the data and variable p_r containing the estimation error.

Chapter 6: PATIENT DATABASE

FOT respiratory impedance measurements were performed using commercially-available Jaeger MasterScreen IOS made by Viasys Healthcare. This system is volume-calibrated daily using a 3 liter manual air pump, which uses a plunger system much like a syringe; pressure calibrations are done by using a 0.2 kPa/(l/s) reference resistance. The test location's altitude, barometric pressure, ambient temperature and relative humidity information is also inputted to the IOS software package as part of the system's calibration procedure.

6.1 DATA QUALITY CONTROL

To avoid air leaks subjects are asked to use nose clips and keep a tight seal with their lips around a mouthpiece attached to the system. Cheeks were supported by voluntary contraction of the circumoral muscles to decrease the upper airway "shunt" effect present at higher frequencies. In the past patients' were asked to push on their cheeks with the palm of their hands, however this might create a counterproductive mechanical loading on the chest wall (36). Test results were analyzed after test completion and data showing abrupt spikes in reactance at 5 Hz ($Z5$) were rejected as these can indicate a swallow or cough during testing; also rejected were data that showed signs of airflow leakage.

In order to provide an estimated standard error of <10% in impedance measurements, it is recommended that at least 100 FFT analysis per test are made and averaged (36); with IOS 5 FFT analyses are made per second, this implies a minimum test length of 20 s. However, for this research each IOS test duration was usually about 40 – 60 s. Furthermore, replicate testing (usually 3 repeats) was almost always done and all test results were averaged for increased data reliability.

6.2 PATIENT CLASSIFICATION AND DEMOGRAPHICS

A total of 582 volunteers of varied health (NL, ASTH and SAI), age (34.9 years ± 15.6 years), height (172.2 cm ± 17.1 cm) and ethnicity were recruited and tested. Repeat testing was often done; especially in cases were bronchodilator (BD) treatment response was being monitored. Because of this, the actual number of IOS tests analyzed and modeled for this study is 670.

Subjects were diagnosed by expert clinicians and classified as one of the following: Normal (NL) respiratory function, possible small airway impairment (PSAI), asthmatics (ASTH), COPD and those suffering from fibrosis. Previous studies have shown that NL and PSAI subjects present similar IOS parameters (48), therefore in this study PSAI subjects were considered as part of the NL group for statistical analysis. Similarly, subjects diagnosed as suffering from either COPD or fibrosis were classified in one group referred to in this study SAI subjects.

6.2.1 Normal

This group consists of 45 Swedish children (height: 158.4 cm ± 16.7 cm, age information not available), classified as either NL or PSAI, 7 US children (height: 155.7 cm ± 22.7 cm, age: 12.4 years ± 3.8 years) with repeat testing 2 years later for a total of 59 IOS tests of children. Also included are 408 Australian firefighters (height: 180.3 cm ± 6.2 cm, age: 43.9 years ± 8.3 years) classified as having normal respiratory function. Table 6-1 shows a summary of relevant demographic data for the NL group.

Table 6-1: Demographic data for both children and adult subjects classified as having normal (NL) respiratory function.

DEMOGRAPHICS - NORMAL		
	Age (years)	***Height (cm)***
Mean	39.7	177.8
S.D.	13.3	10.7
Number of IOS Tests		
467		

6.2.2 Asthmatics

This group consists of 21 adult subjects (height: 170.1 cm ± 9.0 cm, age: 34.6 years ± 9.4 years) with repeat testing for BD response, for a total of 42 IOS tests of adult asthmatics. Also classified as asthmatics were 12 children (height: 130.5 cm ± 15.8 cm, age: 8 years ± 2.3 years), all of whom were submitted to repeat testing 2 years later for BD response for a total of 36 tests of asthmatic children. Table 6-2 shows relevant demographic data for the asthmatic subjects. All tests in this classification were collected from US volunteers.

Table 6-2: Demographic data for both children and adult subjects classified as having asthmatic (ASTH) respiratory function.

DEMOGRAPHICS - ASTHMATICS		
	Age (years)	***Height (cm)***
Mean	20.4	148.9
S.D.	14.8	23.4
Number of IOS Tests		
Pre-BD	**Post-BD**	**Total**
45	33	78

6.2.3 Small Airway Impairment

Included in the SAI group are 7 US children (height: 125.6 cm ± 14.1 cm, age: 8 years ± 2.2 years) that submitted to repeat testing 2 years later for BD response, 10 Swedish children (height: 141.7 cm ± 14.9 cm, no age information available) all of whom were tested pre-BD and post-BD administration; a total of 41 tests were done on children classified as having small airway impairment. The adult subjects in this group are 28 Australian firefighters (height: 178.4 cm ± 6.3 cm, age: 43.9 years ± 7.1 years) and 56 subjects from the UK (height: 169.2cm ± 10cm, no age information available) diagnosed with fibrosis. Table 6-3 shows relevant demographic data for subjects in this particular data set.

Table 6-3: Demographic data for both children and adult subjects classified as having asthmatic (ASTH) respiratory function.

DEMOGRAPHICS - SAI		
	Age (years)	***Height (cm)***
Mean	32.3	163.4
S.D.	17.7	19.0
Number of IOS Tests		
Pre-BD	**Post-BD**	**Total**
108	17	125

Chapter 7: MEAD'S MODEL CIRCUIT ANALYSIS

As previously mentioned, extensive attempts have been made to estimate respiratory impedance data using different configurations of electric circuit models. Mead's respiratory impedance model has traditionally provided the best fit and parameters estimations to observed FOT data. However, recent attempts at modeling IOS data using Mead's model have resulted in less-than optimal estimations. While Mead's model provides excellent data fit, it has been reported that, when using IOS data, estimated impedance calculations have yielded parameter values for lung-tissue compliance (C_l) and chest-wall (C_w) compliance too large to be physiologically realistic (10). In fact, the obtained parameter values are sometimes too large by several orders of magnitude, for all intents and purposes short-circuiting those elements from the circuit.

Taking a small arbitrary sample of 15 Swedish children classified as NL (height: 158.7 cm ± 18.3 cm, age information not available), the algorithm described in Chapter 5: was used to estimate parameters for Mead's model. The results are summarized in Table 7-1, in it one can see that setting upper boundaries for C_l and C_w results in somewhat reasonable average values for those parameters. However, looking at results obtained when no upper boundaries are set it is clear that average and standard deviations are too large by several orders of magnitude for both parameter values. This suggests that both parameters very often reach the upper constraints, and in fact, even when upper constraints were set C_w reaches the upper boundary for almost half of the subjects (7 out of 15 estimated) and C_l almost always reached the upper boundary (7 out of 15 estimated).

Table 7-1: Estimated parameters for 15 random NL Swedish children using Mead's Model with and without upper boundaries set for C_l and C_w.

ESTIMATED PARAMETERS FOR 15 NL CHILDREN USING MEAD'S MODEL							
				Mead			
	Rp	R	Cl	Cp	Cw	Ce	I
Mean (Cl, Cw < 2)	0.344	0.343	1.700	0.201	1.544	0.001	0.002
S.D.	0.142	0.085	0.649	0.123	0.643	0.001	0.001
Mean	0.377	0.350	6192.832	0.186	905.771	0.001	0.002
S.D.	0.159	0.080	4773.753	0.102	2828.180	0.001	0.001

7.1 PROPOSED PROBLEM ORIGIN

IOS test results by themselves have been proven to provide good measurements of respiratory function and in general, Mead's Model itself is generally regarded as providing good results for FOT impedance modeling. Moreover, numerical estimation techniques have improved due to constant research done on this topic over the years. All of this suggests that Mead's model could be inappropriate for IOS data in particular.

It can be reasoned that this model behavior results from the very small volume displacements produced by IOS, which are usually in the 5 to 10 ml range. Such volumes by themselves can be considered to be very small compared to lung volume (~4 l); unlike impulses, other excitation signals such as the sinusoidal oscillations used by Mead use larger air volumes to stimulate the respiratory system, it would not be uncommon to use volumes 10 times larger than those produced by IOS (47). If one adds the fact that most FOT signal energy is dissipated in the upper airways then it is not unreasonable to assume that unlike other FOT techniques that use IOS impulses has a negligible effect on the subject's lung tissue and chest wall. If this assumption is correct than it would mean that Mead's model contains parameters that seek estimate properties in regions of the respiratory system that IOS fails to stimulate; making C_l and C_w dispensable in this study.

In order to provide evidence towards this dispensable nature of the mentioned parameters a circuit analysis was performed, the reasoning being that simulating the effect that IOS stimuli has on Mead's model provides insight into its behavior. The methods and some results of this analysis were previously published by this author along with contributors (43), (44), however here it is presented more extensively and in-depth, collecting and updating information presented in those publications.

7.2 WORKING WITH MEAD'S MODEL

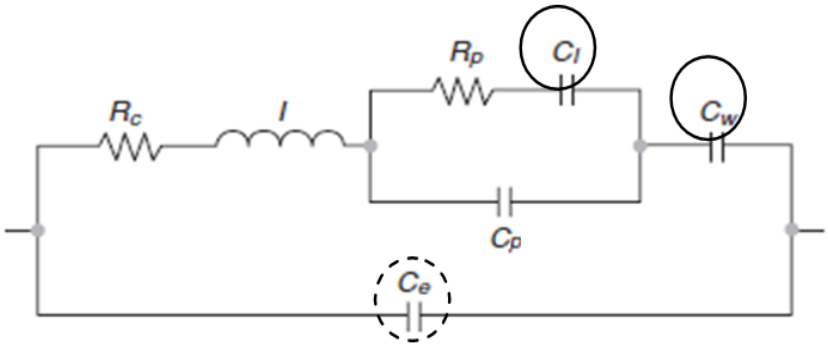

Figure 7-1: Mead's Model of human respiratory impedance, deleting parameters marked with solid-line circles results in the aRIC Model, further removing the parameter denoted by the dashed circle results in the eRIC Model.

This model, here shown in Figure 7-1 and better described in section 4.3, is described by impedance equations that are complex in nature:

$$(7\text{-}1) \quad Z = \frac{-j}{\omega C_e} || Z_m$$

Where:

$$(7\text{-}2) \quad Z_m = \frac{R_p {C_l}^2}{\omega^2 {R_p}^2 {C_p}^2 {C_l}^2 + (C_p + C_l)^2} + R_c + j\left(-\frac{\omega^2 {R_p}^2 {C_p}^2 {C_l}^2 + C_p + C_l}{\omega\left[\omega^2 {R_p}^2 {C_p}^2 {C_l}^2 + (C_p + C_l)^2\right]} + I - \frac{1}{\omega C_w}\right) = R_m + jX_m$$

And so:

(7-3) $$Z_R = Re(Z) = \frac{R_m}{1-2\omega C_e X_m+\omega^2 {C_e}^2({R_m}^2+{X_m}^2)}$$

(7-4) $$Z_X = Im(Z) = \frac{X_m-\omega C_e({R_m}^2+{X_m}^2)}{1-2\omega C_e X_m+\omega^2 {C_e}^2({R_m}^2+{X_m}^2)}$$

It is obvious by looking at equations (7-1) to (7-4) that there is an increased level of difficulty associated with working with these impedance equations. This is due both to their complex nature and their large number of parameters, for this reason *Mathematica* software package was chosen to work with closed form equations, while *Matlab* was utilized for further calculations and plots.

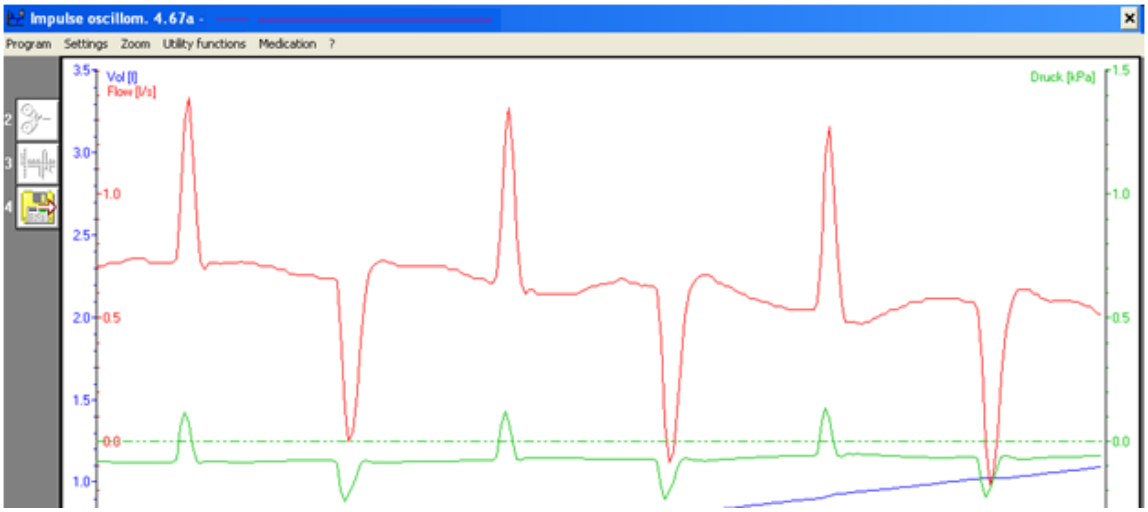

Figure 7-2: Part of a screenshot taken during IOS testing of a NL adult subject (height: 172 cm, age: 55).

IOS input flow is considered to be aperiodic and pulsatile, as such, a single impulse analysis of the circuit is presented here. Input flow $F_s(t)$ to the model was approximated in a manner which would closely resemble an actual input flow pulse, while still being practical to work with using Laplace transformations. This approximation is shown in eqn. (7-5).

(7-5) $$F_s(t) = 0.7UnitTriangle[100/3(t-1/50)]sine(20\pi t) - 0.1UnitTrangle[200/3(t-0.03-1/50)]sine[50/3\,\pi(t-.04)]$$

It can be seen in Figure 7-2: Part of a screenshot taken during IOS testing of a NL adult subject (height: 172 cm, age: 55).Figure 7-2 that IOS develops roughly triangle-shaped 60-70 ms waveforms for pressure and flow, which is represented in eqn. (7-5) by the triangle function (UnitTriangle[]) However, to better approximate the input flow and still be practical to use with Laplace transformations some sinusoidal components were added. Figure 7-3 shows the approximated flow waveform along with the calculated resulting pressure across the circuit.

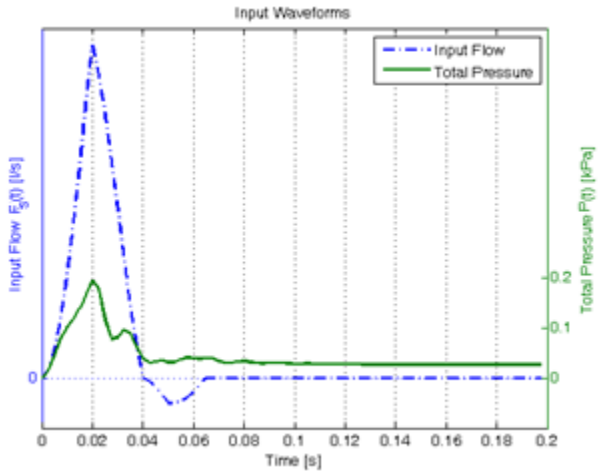

Figure 7-3: Approximated input flow impulse ($F_s(t)$) used in circuit analysis of the Mead's respiratory impedance model and calculated total available pressure ($P(t)$) for the normal adult patient

The area under $F_s(t)$ can be calculated by integrating the input waveform with an upper limit of 200 ms, corresponding to an oscillation frequency of 5 Hz, as used in IOS measurements. This is illustrated in eq. (7-6), which shows that in this simulation the model receives a total input air volume of approximately 16 ml; an adequate representative volume for purposes of this analysis, only slightly larger than typical IOS displacement volumes.

$$\int_0^{0.2} F_s(t)d(t) = 0.01638\ liters. \quad (7\text{-}6)$$

7.2.1 Data sample

A varied and large sample from the database described in chapter 6 was used to calculate model parameters for this circuit analysis. This analysis used the following data: 7 US children (height: 155.7 cm ± 22.7 cm, age: 12.4 years ± 3.8 years) classified NL all of whom with the exception of one came in for repeat testing for pre-BD and post-BD response giving a total of 22 datasets, 45 NL Swedish children (height: 158.4 cm ± 16.7 cm, age information not available), 21 US adult ASTH (height: 170.1 cm ± 9.0 cm, age: 34.6 years ± 9.4 years) all of whom had post-BD data as well as inspiratory-only data for a total of 84 datasets, 12 children from the US with ASTH (height: 130.5 cm ± 15.8 cm, age: 8 years ± 2.3 years) with repeat testing 2 years later for both pre-BD and post-BD treatment response resulting in 36 datasets, 10 Swedish children (height: 141.7 cm ± 14.9 cm, no age information available) diagnosed with SAI, of whom 8 had post-BD data and all had inspiratory-only data for a total of 36 datasets, 7 US children (height: 125.6 cm ± 14.1 cm, age: 8 years ± 2.2 years) were classified as SAI and were subjected to repeat testing for pre-BD and post-BD response giving a total of 21 datasets and lastly, 56 adolescent and young adult subjects (height: 163.2cm ± 10cm, no age information available) from the UK classified in the SAI group.

The database therefore consisted of a total of 300 distinct test results (height: 155.8 cm ± 20.2 cm, age: 17.3 years ± 9.1 years); Mead model parameters were estimated for each test result using the algorithm described in Chapter 5: with upper constraints set for C_l and C_w.

7.3 LAPLACE CIRCUIT ANALYSIS

For the analysis done in this paper, impedances of Mead's model parameters were represented in the *s*-domain corresponding to their Laplace transformation as: $Z_I = sI$, $Z_{Cl} = 1/sC_l$, $Z_{Cp} = 1/sC_p$, $Z_{Cw} = 1/sC_w$ and $Z_{Ce} = 1/sC_e$.

Similarly, the input flow $F_s(t)$ was transformed to the *s*-domain using Laplace transformation, represented by $F_s(s) = L\{F_s(t)\}$.

Because of the degree of difficulty and the complex nature of the equations being used numerical results are generally complex and non-descriptive and are therefore not presented here; instead plots and tables illustrating the model's behavior will be included in this analysis. Using Laplace transformations greatly simplifies the circuit analysis, for example, to obtain the pressure drop due to inertance it is simply a matter of calculating the *s*-domain flow through *I*, applying Ohm's Law to obtain the *s*-domain pressure drop and then converting back to time-domain using an inverse Laplace transformation ($L^{-1}\{\ \}$). This process is illustrated in the following steps:

$$P_I(t) = L^{-1}\{F(s)[Z_{Ce}/(Z_{Ce} + Z_1)]\, Z_I\} \tag{7-7}$$

Where Z_1 the total impedance is created by the R_c, I, R_p, C_l, C_p and C_w parameters and is calculated as follows:

$$Z_1 = R_c + Z_l + \left[(Z_{Cl} + R_p) \,||\, Z_{Cp}\right] + Z_{Cw} \tag{7-8}$$

Here, $[(Z_{Cl} + R_p) \,||\, Z_{Cp}]$ is the equivalent impedance created by the combination of R_p, C_l, and C_p. The following values were obtained and used for one normal adult patient (height: 172 cm, age: 55): R_c = *.16202, I = .00110,* R_p *= .11479,* C_p *= .24167,* C_e *= .00412,* C_l *= 1.21740* and C_w *= 1.03680*, with units of kPa/(l/s), kPa/(l/s^2) and l/kPa for resistance, inertance and compliance, respectively. Using the normal adult's parameter values and applying them to eqn. (7-7) the result was then plotted and is shown in Figure 7-4 along with the calculated pressure drop across R_c.

Similarly, all other pressure drops for the normal adult patient were calculated and plotted in figures , the outstanding feature is the very small pressure drops across C_l ($P_{Cl}(t)$) and C_w,($P_{Cw}(t)$), which

are plotted in this figure . To further clarify how small these contributions are, calculated maximum values of $P(t)$, $P_{Cl}(t)$and $P_{Cw}(t)$ are: $P \approx 0.1967\ kPa$, $P_{Cl,max} \approx 0.0110\ kPa$, and $P_{Cw,max} \approx 0.0163\ kPa$. Thus, contributions to total max pressure drop are approximately 5.7% by C_l and 8.3% for C_w.

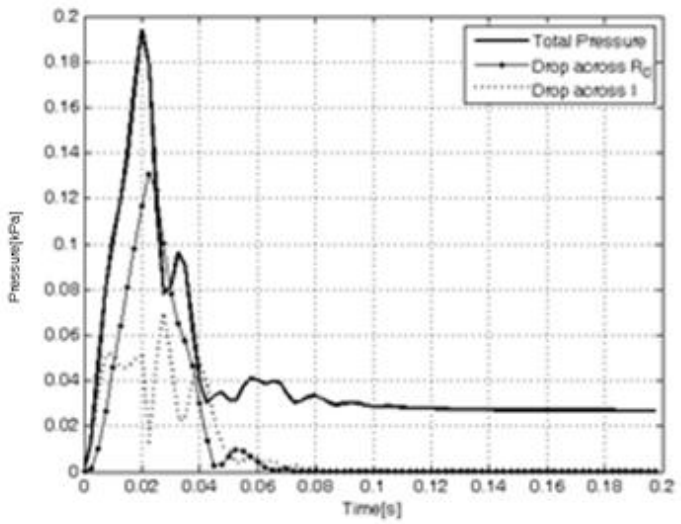

Figure 7-4: Simulated pressure drop across Mead's model elements R_c and I, calculated using parameter values obtained for one normal adult subject.

The calculated pressure and flow waveforms provide enough information to calculate the *energy dissipated* at each parameter in the following manner:

(7-9) $E = \int_0^{0.2} P_\theta(t)\, f_\theta(t) dt$ Where θ is the parameter of interest (i.e. $P_R(t)$ is the pressure drop across upper airway resistance R_c).

Energy dissipations at parameters R, I, R_p, C_l, C_p and C_w were calculated and are presented in Table 7-2 for the normal adult.

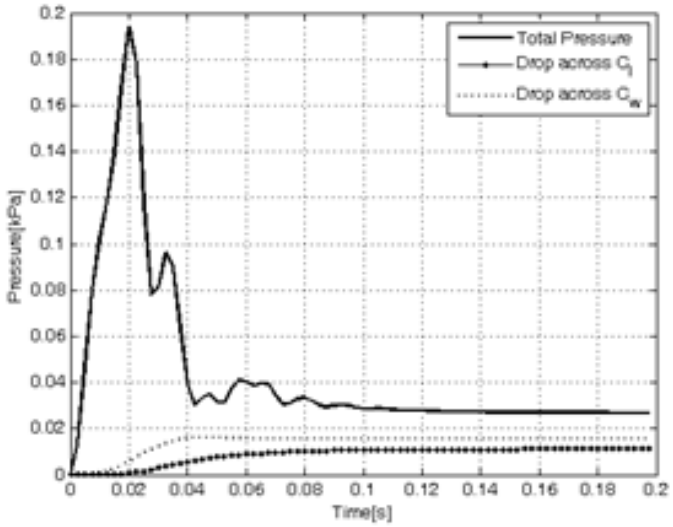

Figure 7-5: Simulated pressure drop across Mead's model elements C_l and C_w, calculated using parameter values obtained for one normal adult subject.

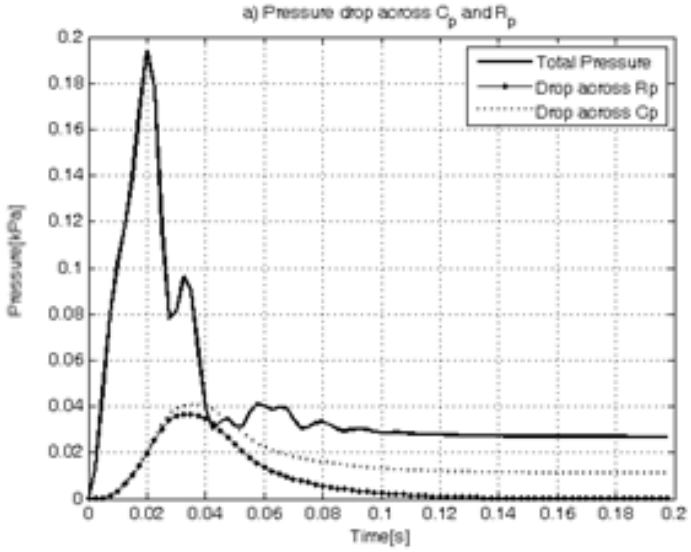

Figure 7-6: Simulated pressure drop across Mead Model elements R_p and C_p, calculated using parameter values obtained for one normal adult subject.

Table 7-2: Energy dissipated across each circuit element for IOS data from one NL adult subject.

	Energy Dissipated (micro Joules)	*Percentage of Total (%)*
Total - Ce	2.163	-
R	1.489	68.9
I	0.127	5.9
Rp	0.327	15.1
Cl	0.076	3.5
Cp	0.015	0.69
Cw	0.128	5.9

Another way in which these calculated pressure waveforms can be appreciated is by integrating them with respect to time, which was done as shown in eq. (7-10).

(7-10) $$A_{p\theta} = \int_0^{0.2} P_\theta(t)\, dt$$

Table 7-3: Values of pressure drop across each circuit element, integrated with respect to time for IOS data from one NL adult (height: 172 cm, age: 55).

	*Integrated Pressure drop (kPa*s)*	*Percentage of Total (%)*
Total	0.0052	-
Rc	0.0026	51.1
I	5.5×10^{-9}	~ 0
Rp	0.0016	30.2
Cl	0.0003	4.8
Cp	0.0018	35.0
Cw	0.0007	13.9

This provided a measure of their total pressure drop. These results are shown in table Table 7-3: Values of pressure drop across each circuit element, integrated with respect to time for IOS data from one NL adult

(height: 172 cm, age: 55). for one normal adult subject. Table 7-2 and Table 7-3 further illustrate the small pressure drops across parameters C_l and C_w with an area of only ~5% and ~14% of the total pressure integral for the normal adult data and with similar results for IOS data from all other subjects.

7.4 RESULTS

Using the same approach taken with the NL adult subject as described in section 7.3 relevant data was calculated for the complete data sample. No significant difference was found when comparing pre-BD and post-BD circuit analysis results for modeling purposes and therefore they were grouped together. Notice, also in Table 7-4 that the pressure dissipated by *Cl* and *Cw* from one respiratory condition to another are very similar, this is also true for all other results and therefore only the total averages are presented in tables Table 7-5 and Table 7-6.

Results for all other subjects showed similar outcomes in all areas, where C_l and C_w contributed only an average of 3.39% and 7.99% respectively compared to total max pressure drop.

Simulations consistently demonstrated that much of the available pressure was dropped across R_c, large airway resistance. Furthermore, the small contribution from C_l makes the contributions from R_p and C_p nearly identical. Analysis using parameter values for C_l and C_w obtained by running the estimation algorithm without upper constraints showed that the pressure drops across these parameters decrease to nearly zero. This may actually be the case in real subjects, as the pressure transmitted by the small impulse signal to the patients' lung tissue and chest wall is likely negligible.

Energy and integrated pressure were also very small across C_l and C_w. Table 7-5 shows that energy dissipation was consistently small across those parameters; lung compliance contributed an average of only 2.1%, while chest wall compliance contributed an average of only 4.9% of total energy dissipated through the model. Table 7-6 shows that for integrated pressure C_l had an average contribution of only 2.1% of total integrated pressure, with only 4.9% for C_w. This shows that even though the pressure

drop across those parameters during steady-state seems to become relevant they are insignificant in the overall contribution to the total effort variable stimulating the respiratory system.

Table 7-4: Mean and standard deviation values of max instantaneous pressure drop across C_l and C_w for the complete (300 dataset) sample arranged by classification. The total pressure drop value excludes pressure drop across C_e.

MEAN MAX INSTANTANEOUS PRESSURE DROP (kPa)					
	Total - Ce	***Cl***	***% of total***	***Cw***	***% of total***
			NL		
Mean	0.328	0.012	3.762	0.020	5.871
Std. Dev.	0.079	0.010	3.899	0.017	3.832
			ASTH		
Mean	0.312	0.011	3.629	0.026	8.265
Std. Dev.	0.073	0.008	2.477	0.020	5.664
			SAI		
Mean	0.348	0.009	2.682	0.030	8.493
Std. Dev.	0.069	0.007	1.927	0.022	5.620
			TOTAL AVERAGE		
Mean	0.320	0.010	3.393	0.026	7.992
Std. Dev.	0.072	0.008	2.665	0.020	5.467

Table 7-5: Mean and standard deviation values of energy dissipation across C_l and C_w for the complete (300 dataset) sample. The total pressure drop value excludes pressure drop across C_e.

AVERAGE ENERGY DISSIPATION (micro Joules)					
	Total - Ce	***Cl***	***% of total***	***Cw***	***% of total***
			TOTAL AVERAGE		
Average	0.008	0.000	2.108	0.000	4.981
Std. Dev.	0.020	0.001	1.408	0.000	3.453

Table 7-6: Mean and standard deviation values of integrated pressure drop across C_l and C_w for all patients. The total pressure drop value excludes pressure drop across C_e.

AVERAGE INTEGRATED PRESSURE DROP (kPa*S)					
	Total - Ce	*Cl*	*% of total*	*Cw*	*% of total*
		TOTAL AVERAGE			
Average	0.008	0.000	2.108	0.000	4.981
Std. Dev.	0.020	0.001	1.408	0.000	3.453

7.5 DISCUSSION

The results above are consistent with the direct pressure measurements of Macklem and Mead (34), which showed that oscillatory pressures delivered to the trachea were 80 to 100 % dissipated as measured by catheters placed in 2 mm diameter airways. Attempts at Mead model parameter estimation using IOS data and no upper constraints during optimization have routinely yielded physiologically unrealistic values for C_l and C_w. Moreover, constrained optimization can be implemented using physiologically sensible values for C_l and C_w, with little to no effect on total error in estimation, providing a strong suggestion of their triviality. It is not unlikely that the very large (and physiologically unrealistic) parameter values are actually a better representation of the insensitivity of the chest wall and lung tissue to IOS stimulus, since large values effectively short-circuit and eliminate their respective parameters from the circuit model.

The circuit analysis presented in this chapter further validates the assumption that chest wall and lung tissue compliance could be ignored when using IOS data, by showing both the inconsequential pressures available at those sites even when using realistic values of driving pressures and airway resistances. If C_l and C_w were to be deleted from the model the resulting five-parameter model would be the *aRIC* model; upon further parameter reduction done by additionally eliminating extra-thoracic compliance (C_e) the resulting four-parameter model would be the *eRIC* model. Both models have recently shown to consistently provide a very small error in estimation and relevant parameter values for diagnosis, many times without the need of constraints (10), (28), (29), (41), (44), (45), (48) (49).

For the reasons stated in this chapter, this thesis focuses on the *aRIC* and *eRIC* models. Chapter 8 will provide a brief description of the modeling results and errors for each model and each type of health classification and chapter 9 will explore the clinical significance of the obtained parameters.

Chapter 8: MODEL PARAMETER ESTIMATION RESULTS

In order for it to be considered effective, a data estimation model must provide a good fit between experimental data and modeled results. One way of measuring experimental and modeled data fit is by calculating the Mean Absolute Error (MAE) of the estimation result. MEA is obtained by finding the average of the absolute value of residual function described in section 5.1. This measure is described in equation (8-1).

(8-1) $MAE = \frac{1}{n}\sum_{i=5}^{25}|r_i(\boldsymbol{p})|$ Where $i = 5, 10, \ldots, 25$; the discrete frequency points, $n =$ the number of measured data points and $\boldsymbol{p}$ is the vector containing the estimated model parameters.

In other words, MAE describes the distance that is to be expected between measured data and estimated data for each frequency point. Throughout this research each dataset contained 5 discrete frequency points for estimation: 5, 10, 15, 20 and 25 Hz. Each dataset contains both resistive and reactive information for every frequency point, therefore the number of data points to be estimated each time is 10. So in the MAE equation ((8-1)) the number of measured data points is $n = 10$.

The mean absolute error was calculated for each data set used in parameter estimation, those values were then arranged and classified according to the subject's health classification: NL, ASTH and SAI. The average and standard deviation of the calculated MAE can be found in Table 8-1 for all NL subjects, Table 8-3 for all ASTH subjects and Table 8-4 for subjects classified in the SAI group.

Table 8-1: Average MAE for all NL subjects and both the aRIC and eRIC models.

MEAN ABSOLUTE ERROR - NL		
	aRIC	*eRIC*
Mean	0.005	0.007
S.D.	0.003	0.003

Table 8-1 means that for a given NL subject, on average, at each frequency point the difference between measured data and its estimated value will be .004 for the aRIC model and .006 for the eRIC model. This can be visualized more clearly by looking at Table 8-2 and figures Figure 8-1 and Figure 8-2. Table 8-2 lists the impedance as measured by IOS, and the estimated impedance values and MAE for both the aRIC and eRIC model. By comparing the MAE with measured values one can conclude that average MAE errors are very small, this conclusion is supported by observing figures 8-1 and 8-2: a small discrepancy can be seen between measured and estimated resistance, however the error in estimated reactance is almost negligible. Also worth noting is the minimum difference in estimations between both models, this suggests that in spite of the difference in MAE (about a 100% increase in MAE for NL subjects from eRIC to aRIC, but still very small), both aRIC and eRIC models fit impedance data very well.

Table 8-2: Measured and estimated impedance for one adult NL subject (height: 183 cm, age: 44 years) along with the MAE for both aRIC and eRIC models.

MEASURED AND ESTIMATED IMPEDANCE FOR ONE NL ADULT SUBJECT											
	R5	***R10***	***R15***	***R20***	***R25***	***X5***	***X10***	***X15***	***X20***	***X25***	***MAE***
Measured	0.26	0.25	0.23	0.25	0.27	-0.07	0.00	0.04	0.08	0.11	
aRIC Estimation	0.262	0.239	0.241	0.251	0.267	-0.069	-0.002	0.041	0.078	0.112	0.004
eRIC Estimation	0.258	0.252	0.250	0.250	0.250	-0.072	0.002	0.044	0.078	0.109	0.006

The observations made regarding NL data fit are also true for those cases were abnormalities in respiratory impedance are present. Although average MAE values for ASTH and SAI subjects seem more significant than for NL subjects plotting measured and estimated impedance for ASTH and SAI subjects shows that data fit by the models is still very good and the difference in estimated impedance between both models is still almost negligible. This can be observed in figures Figure 8-3 and Figure 8-4, which show IOS and estimated impedance for both aRIC and eRIC models using data from a typical SAI subject (height: 180 cm, age: 22 years).

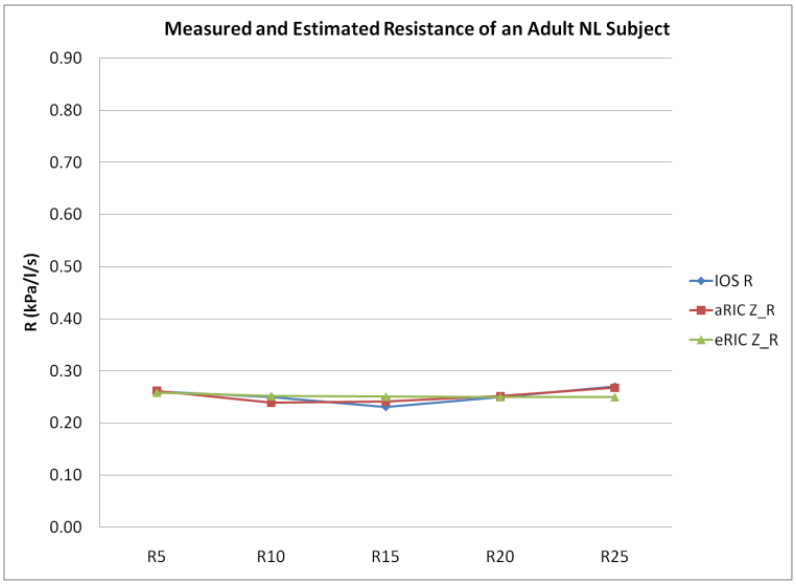

Figure 8-1: Plot of Resistance (R) as measured by IOS and estimated by both aRIC and eRIC models. Data from one adult NL subject (height: 183 cm, age: 44 years) with MAE of 0.004 for aRIC and 0.006 for eRIC.

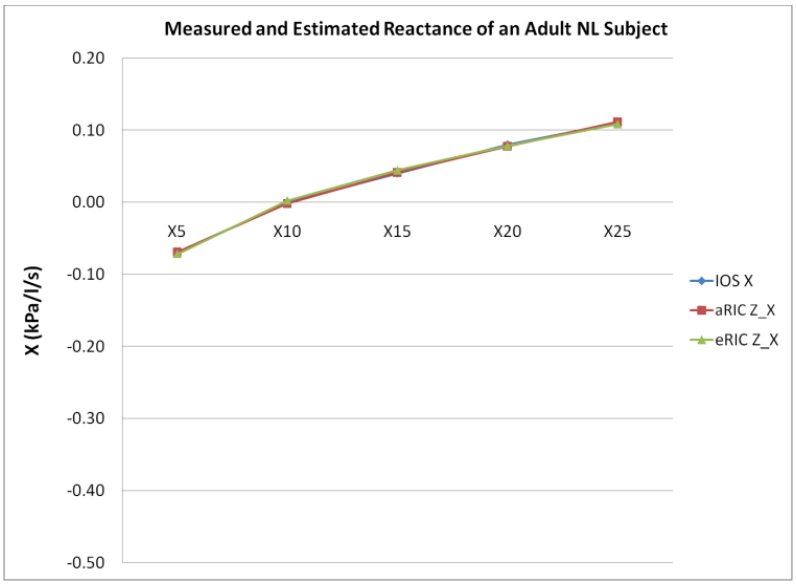

Figure 8-2: Plot of Reactance (X) as measured by IOS and estimated by both aRIC and eRIC models. Data from one adult NL subject (height: 183 cm, age: 44 years) with MAE of 0.004 for aRIC and 0.006 for eRIC.

Table 8-3: Average MAE for all ASTH subjects and both the aRIC and eRIC models.

MEAN ABSOULUTE ERROR - ASTH		
	aRIC	***eRIC***
Mean	0.018	0.024
S.D.	0.007	0.010

Table 8-4: Average MAE for all SAI subjects and both the aRIC and eRIC models.

MEAN ABSOLUTE ERROR - SAI		
	aRIC	***eRIC***
Mean	0.015	0.024
S.D.	0.009	0.019

While previous reports have shown that, although Mead's model outperforms both the aRIC and eRIC models in terms of mean estimation error, those same reports conclude that both aRIC and eRIC still provide more than adequate data fit (10), (45). Furthermore, as can be seen in Figure 8-5, there is a close correspondence between the two models' estimates of C_p (slope = 0.94, with r = 0.99). In the same way, close correspondence for models' estimates of R_c (slope = 0.96 and r = 0.91) and I were found (slope = 1.48 and r = 0.89). Previous publications had shown similarly close model estimates for R_p using SAI and ASTH data (30), which is also true in this study when excluding NL data (slope = .65 and r = 0.82). However, once NL data is included, the correspondence between models' estimated of R_p is not significant (slope = .09, with r = .23). If good correspondence between models' estimated values for R_p had been found for all subjects then it could be concluded that there is no need to use the aRIC model, since C_e offers no diagnostic value, it is merely meant to simulate upper airway shunt compliance. However, estimated values for R_p obtained using the eRIC model are significantly higher than those obtained with the aRIC model, which will be explored in the next chapter along with the clinical significance to model estimated parameters.

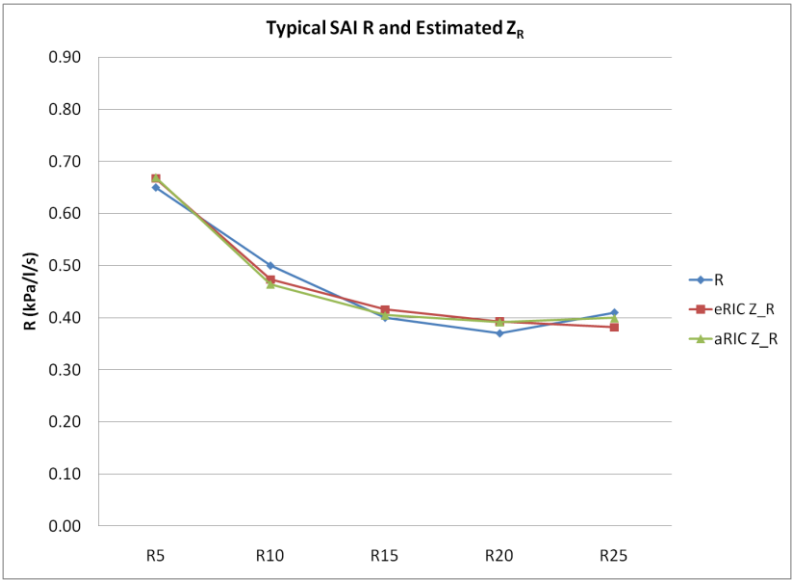

Figure 8-3: Resistance (R) as measured by IOS and as estimated by aRIC and eRIC models. Data from one adult SAI subject (height: 180 cm, age: 22 years) with aRIC MAE = 0.016 and eRIC MAE = 0.021.

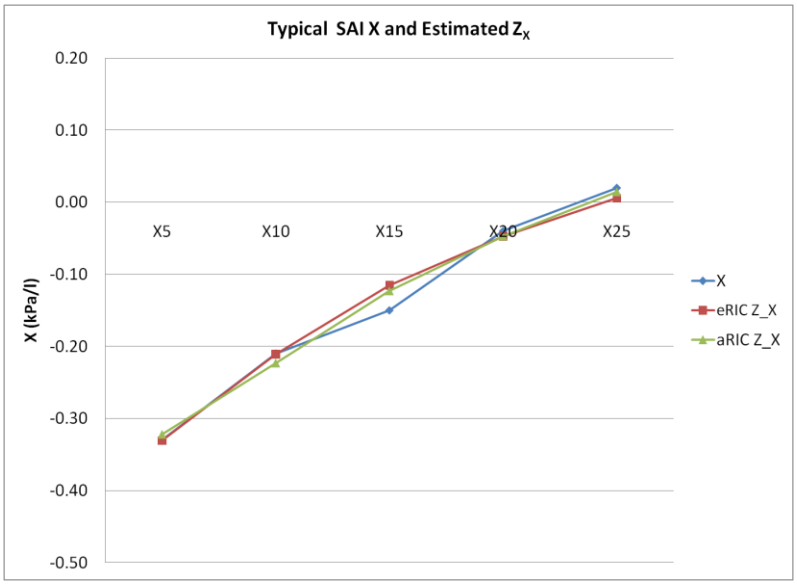

Figure 8-4: Reactance (X) as measured by IOS and as estimated the aRIC and eRIC models. Data from one adult SAI subject (height: 180 cm, age: 22 years) with aRIC MAE = 0.016 and eRIC MAE = 0.021.

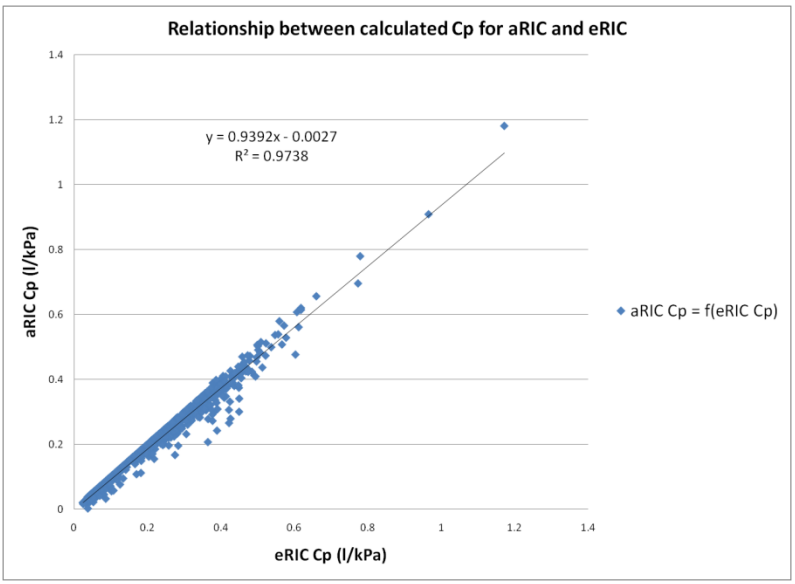

Figure 8-5: Relationship between the models' estimated parameter Cp for all subjects. In general there is a similar correspondence between all model estimated parameters.

Chapter 9: CLINICAL RELEVANCE OF MODEL PARAMETERS

The resistive component of respiratory impedance (R) includes central and peripheral airways, lung tissue and chest wall resistance. It has been shown by direct pressure measurements that central resistance dominates (34) and lung tissue and chest wall resistance are negligible (36). In healthy subjects, R is almost constant except at higher frequencies due to upper airway shunt effect, airway obstruction either in the proximal or distal airways increases R5 and therefore the region of airway obstruction must be inferred from the overall shape of R (36). In general, proximal airway obstruction elevates R evenly while in peripheral airway obstruction R is highest at low frequencies and diminishes as frequency increases.

This effect, now know as negative frequency-dependence of R (fdR), has been shown to closely reflect peripheral airway obstruction (28), (36), (34), (44), (48). Beyond experimental observations negative fdR can be explained in terms of time-constants (47). A tissue's time constant is the product of its resistance and compliance, it's measured in seconds and it describes how fast a tissue can react to stimuli, i.e. the smaller the time constant the faster the tissue can react to stimuli. The lung periphery must be more compliant and offer higher airflow resistance than proximal airways; it must therefore have a larger time constant and its ability to respond to high frequency stimuli is less than that of the central airways. An increase in peripheral airway resistance will therefore have a more noticeable effect on low frequency resistance as measured by FOT. The effect that peripheral airway obstruction has on resistance (R) can be observed in Figure 9-1 which plots the average impedance measurements for NL, ASHT and SAI subjects, excluding post-BD data.

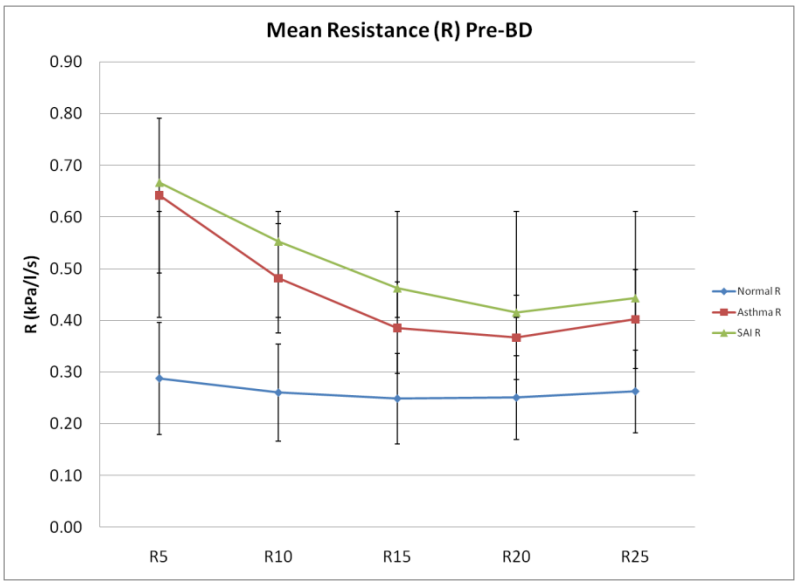

Figure 9-1: Average impedance for all subjects in each health classification excluding post-BD data. Included are standard deviation bars for each frequency point.

The reactive component of impedance includes the inertive and elastic properties of the airways. The nature of reactance is such that when it is measured to be below zero it is because capacitive reactance dominates and when reactance is above zero inertive forces dominate:

(9-1) $X(f) = \omega I - 1/(\omega C)$, where $\omega = 2*\pi*f$.

Peripheral airways are more compliance than central airways, and central airways have a greater inertive force then peripheral airways, low-frequency (below fres) reactance then reflects the system's ability to store capacitive energy. Because of this, integrated low-frequency reactance (AX, previously explained in section 3.3.6) is closely related to peripheral airway compliance and reflects changes in the degree of peripheral airway obstruction (28), (34), (36), (44), (48). The effect that peripheral airway obstruction has on reactive impedance can be observed in figure Figure 9-2 which plots the average impedance for all NL, ASTH and SAI subjects excluding pre-BD data. Notice the increased reactance for patients with ASTH and SAI, especially at lower frequencies.

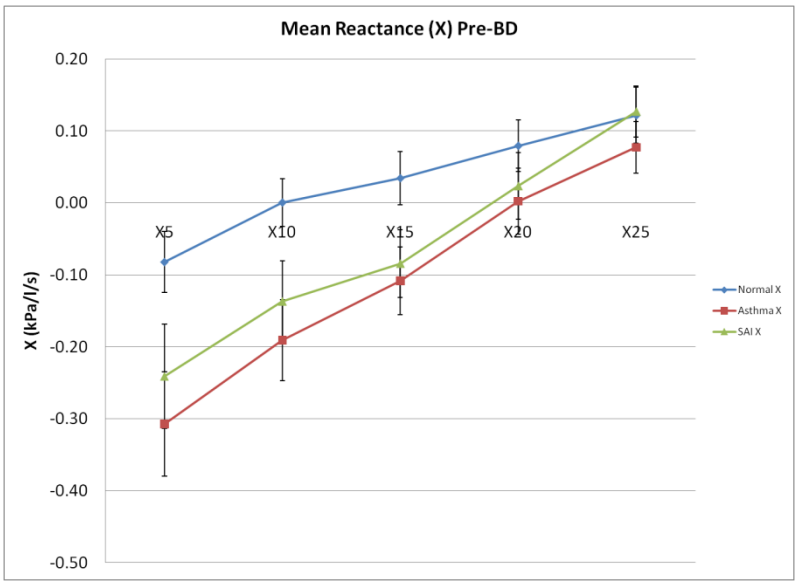

Figure 9-2: Average impedance for all subjects in each health classification excluding post-BD data. Included are standard deviation bars for each frequency point.

For the reasons described above R5, fdR and AX were selected as IOS indices of particular interest, as have been shown to reflect a subject's level of respiratory function. Using information from the database described in chapter 6 those IOS parameters were analyzed to determine if they provide a statistical distinction between NL, ASTH and SAI subjects, this was done using Student's t-test where $p < 0.05$ was considered as significant. The results of these analyses can be seen in tables Table 9-1 and

Table 9-2, which show that there is a significant statistical difference in all cases: AX, fdR and R5 are all markedly different between the NL and ASTH groups as well as between NL and SAI and groups.

For ASTH and SAI subjects that had pre-BD and post-BD measurements, it was found that all IOS indices (AX, fdR and R5) were significantly changed in response to treatment (tables

Table 9-3 and

Table 9-4). As would be expected mean values for all parameters dropped significantly in response to BD administration. It's worth noting that in all cases AX performs better than other IOS indices in reflecting pulmonary function; it distinguishes NL from ASTH and SAI subjects better than fdR and R5, while also showing the best response to BD administration.

Table 9-1: Statistical difference between IOS parameters for all NL and ASTH subjects including post-BD data. A value of $p < 0.05$ means that the difference between measured parameters is significant.

Statistical Difference of IOS Parameters for Normal and Asthmatic Subjects						
	NL AX	***Asth AX***	***NL fdR***	***Asth fdR***	***NL R5***	***Asth R5***
Mean	0.237	2.309	0.037	0.217	0.288	0.642
p -value	**< 0.05**		**< 0.05**		**< 0.05**	

Table 9-2: Statistical difference between IOS parameters for all NL and ASTH subjects including post-BD data. A value of $p < 0.05$ means that the difference between measured parameters is significant.

Statistical Difference of IOS Parameters for Normal and SAI Subjects						
	NL AX	***SAI AX***	***NL fdR***	***SAI fdR***	***NL R5***	***SAI R5***
Mean	0.237	0.899	0.037	0.134	0.288	0.667
p -value	**< 0.05**		**< 0.05**		**< 0.05**	

Table 9-3: IOS parameters for pre-BD and post-BD ASTH data, including the mean values, standard deviation (SD), percent change and statistical significance.

IOS PARAMETERS - ASTHMATICS						
	Pre-BD			*Post-BD*		
	AX	**fdR**	**R5**	**AX**	**fdR**	**R5**
Mean	2.261	0.266	0.616	0.802	0.138	0.415
S.D.	1.359	0.101	0.155	0.638	0.081	0.128
Percent change (%)				-64.5	-48.1	-32.6
p-value				**< 0.05**	**< 0.05**	**< 0.05**

Table 9-4: IOS parameters for pre-BD and post-BD ASTH data, including the mean values, standard deviation (SD), percent change and statistical significance.

IOS PARAMETERS - SAI						
	Pre-BD			*Post-BD*		
	AX	**fdR**	**R5**	**AX**	**fdR**	**R5**
Mean	1.676	0.251	0.667	1.112	0.188	0.561
S.D.	0.674	0.083	0.121	0.632	0.073	0.126
Percent change (%)				-33.7	-25.3	-15.8
p-value				**< 0.05**	**< 0.05**	**< 0.05**

9.1 MODEL-DERIVED PARAMETERS REFLECT IOS INDICES

Previous reports have found close relationships of IOS indices (AX and fdR) to model derived parameters C_p and R_p (29), (41). In the general sense this is also true in this study. When plotting model derived C_p as a function of IOS AX (fig. Figure 9-3: Relationship between models' C_p and measured IOS AX for all subjects.) a very close relationship was found for both models (r = .92 for aRIC and r = .96 for eRIC), with nearly indistinguishable regressions. This is as expected, AX reflects system capacitance particularly in the periphery.

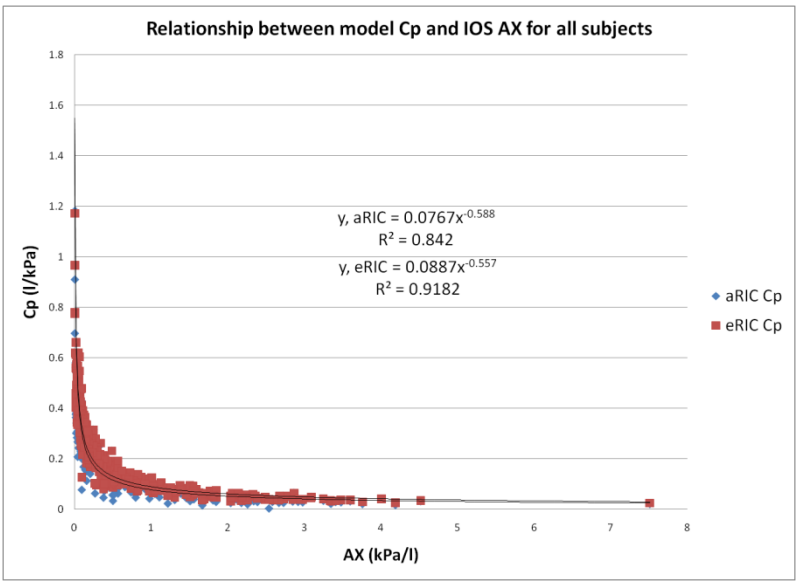

Figure 9-3: Relationship between models' C_p and measured IOS AX for all subjects.

Looking at C_p as a function of fdR there is a similarly good relationship with r = .93 for aRIC and r = .96 for eRIC. For R_c as a function of R5 results in an almost linear relationship, with r = .76 for aRIC and r = 84 for eRIC. On the other hand, R_p doesn't seem to perform nearly as well when plotted as a function of fdR with aRIC r = .5 and eRIC r = .09, there seems to be no relationship between estimated R_p and measured fdR, especially in the case of the eRIC model. However, when removing NL patients the relationship between fdR and R_p improves, with aRIC r = .67 and eRIC r = .47, this improvement is significant especially in the case of the eRIC model. The eRIC model is designed to be able to model IOS measured resistance that contains noticeable negative fdR, in other words, it requires a monotonic decrease in measured R as frequency increases. When using the eRIC model with NL patients that shown little to no fdR the estimates for R_p are often usually high, especially considering NL patients should not present increased peripheral airway resistance.

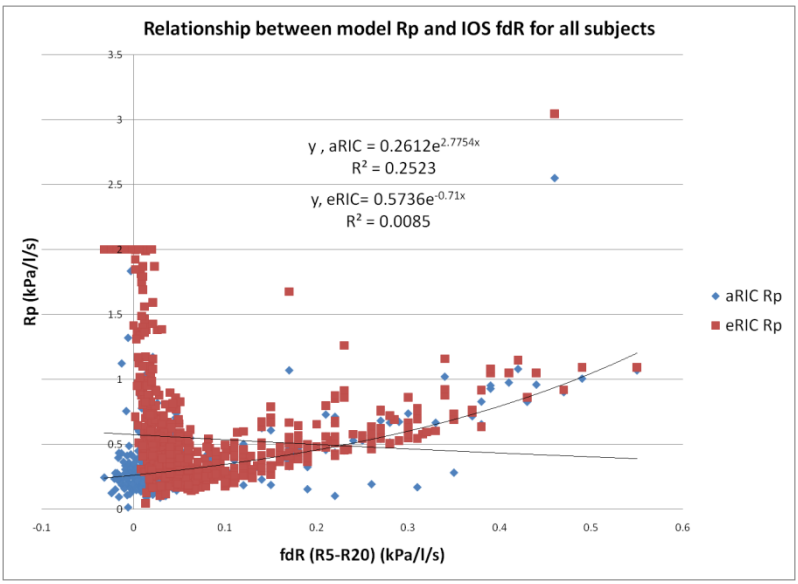

Figure 9-4: Relationship between models' R_p and measured IOS AX for all subjects.

9.2 IOS INDICES TRACK CHANGES IN RESPIRATORY FUNCTION

A subject's IOS indices AX, fdR and R5 are expected to somewhat differ with age and it is not uncommon for normal healthy children to manifest some fdR and larger reactance measurements than normal adults (36). However it has been previously shown, that IOS indices provide good discrimination between NL and SAI children in the same age group over a two-year period (28). That same study showed that although there was an appreciable change in IOS parameters it was only significant for fdR in SAI children. In this particular study, AX, fdR and R5 were all found to be significantly larger in normal children than in normal adults (both with $p < 0.05$). However, comparing NL children to ASTH it was found that only R5 was unable to distinguish NL from SAI children, while all other IOS indices showed marked differences between NL children, and the both the ASTH and SAI groups. Therefore, in

spite of the noticeable differences in IOS parameters between children and adults, most IOS are still able to distinguish healthy from diseased lungs.

IOS has also been proven to show good sensitivity in tracking lung function response to BD treatment. Both resistance and reactance react in a manner that reflects airway improvement after treatment. Overall resistance is decreased as well as fdR, indicating a decrease in peripheral airway resistance. For measured reactance, both X5 and fres show a noticeable decrease from pre- to post-BD treatment. Consequently AX is also decreased (28) (29) (36) (50) (41) (51). Figure 9-5 and Figure 9-6 plot the mean impedance values for those ASTH and SAI patients that received BD treatment. SAI patients were particularly aggravated, and although BD response is noticeable, it is even more so in ASTH patients, which show a very obvious decrease in AX and fdR. Table 9-7 and Table 9-8 illustrate the change in IOS indices in response to BD treatment. All indices showed significant differences in response to BD treatment, with AX being the most sensitive of them.

Table 9-5: Statistical difference between IOS parameters for NL children and ASTH subjects including post-BD data. A value of $p < 0.05$ means that the difference between measured parameters is significant.

Statistical Difference of IOS Parameters for Normal children and Asthmatic Subjects						
	NL Children AX	***All Asth AX***	***NL Children fdR***	***All Asth fdR***	***NL Children R5***	***All Asth R5***
Mean	0.428	2.309	0.079	0.217	0.463	0.642
p -value	**< 0.05**		**< 0.05**		**< 0.05**	

Table 9-6: Statistical difference between IOS parameters for NL children and ASTH subjects including post-BD data. A value of $p < 0.05$ means that the difference between measured parameters is significant.

Statistical Difference of IOS Parameters for Normal children and SAI Subjects						
	NL Children AX	***All SAI AX***	***NL Children fdR***	***All SAI fdR***	***NL Children R5***	***All SAI R5***
Mean	0.428	0.899	0.079	0.134	0.463	0.442
p -value	**< 0.05**		**< 0.05**		> 0.05	

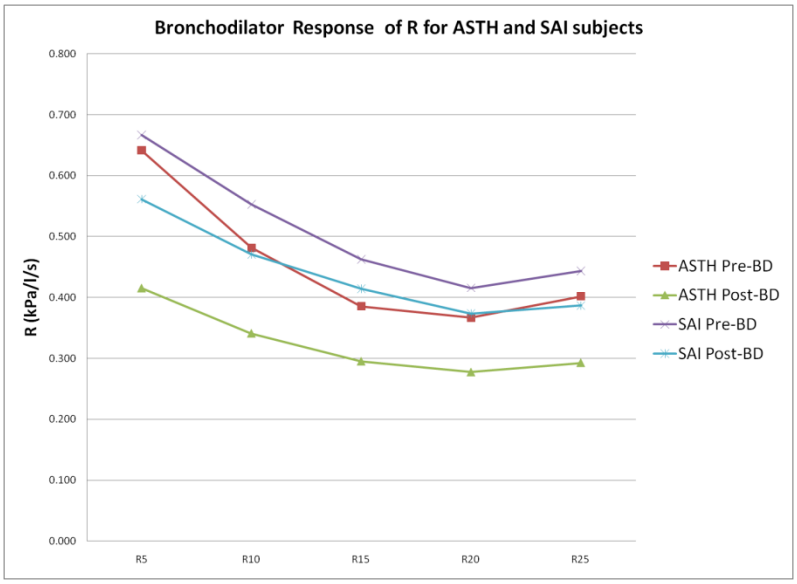

Figure 9-5: Mean resistance (R) for pre-BD and post-BD data from ASTH and SAI subjects.

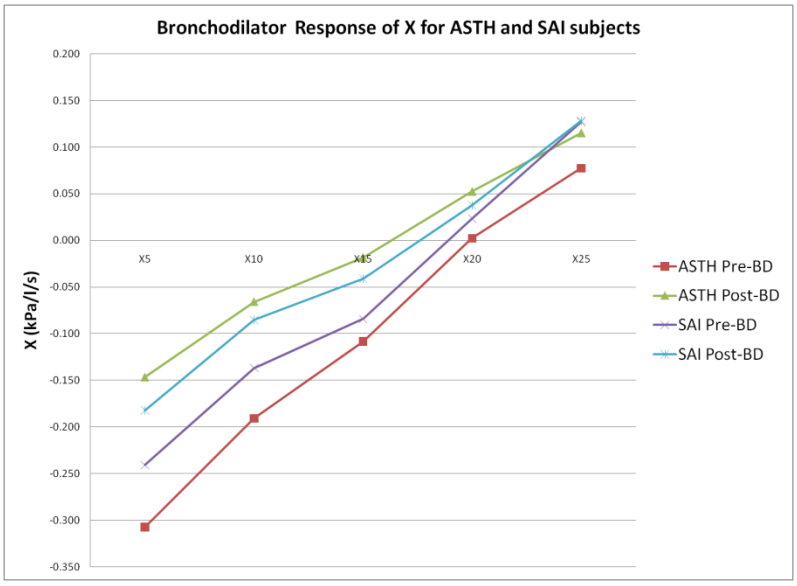

Figure 9-6: Mean reactance (X) for pre-BD and post-BD data from ASTH and SAI subjects.

Table 9-7: IOS indices and their response to BD treatment in ASTH subjects. Their percent change along with the statistical significance is included.

IOS PARAMETERS - ASTHMATICS						
	Pre-BD			*Post-BD*		
	AX	**fdR**	**R5**	**AX**	**fdR**	**R5**
Mean	2.261	0.266	0.616	0.802	0.138	0.415
S.D.	1.359	0.101	0.155	0.638	0.081	0.128
Percent change (%)				-64.5	-48.1	-32.6
p-value				**< 0.05**	**< 0.05**	**< 0.05**

Table 9-8: IOS indices and their response to BD treatment in SAI subjects. Their percent change along with the statistical significance is included.

IOS PARAMETERS - SAI						
	Pre-BD			*Post-BD*		
	AX	**fdR**	**R5**	**AX**	**fdR**	**R5**
Mean	1.676	0.251	0.667	1.112	0.188	0.561
S.D.	0.674	0.083	0.121	0.632	0.073	0.126
Percent change (%)				-33.7	-25.3	-15.8
p-value				**< 0.05**	**< 0.05**	**< 0.05**

9.3 MODEL PARAMETERS REFLECT BRONCHODILATOR RESPONSE

In the general case, obtained model parameters closely reflect IOS indices under normal conditions, as was described in section 9.1. Similarly to IOS indices (AX, fdR and R5) model parameters respond strongly to BD treatment. Table 9-9 shows BD response for both models' parameters in ASTH patients. There is a decrease in R_p much as it happens in the human lung: BD administration increases peripheral airway diameter and therefore peripheral resistance is reduced. The model parameter most sensitive to BD administration is C_p, with much smaller changes for R_c and I, which are also as expected because BD treatment is not meant to target upper airways.

Table 9-10 shows both models' parameter response to BD treatment, similarly to what was observed for ASTH subjects, there is a noticeable decrease in R_p and C_p remains the more sensitive parameter. It's worth noting that C_p demonstrates greater change than even the most sensitive IOS index (AX).

Table 9-9: Estimated models' parameters for ASTH subjects with pre and post-BD IOS measurements. The percent change for each parameter is included.

ESTIMATED PARAMETERS - ASTHMATICS								
Pre-BD								
aRIC					***eRIC***			
Rp	**Rc**	**Cp**	**Ce**	**I**	**Rp**	**Rc**	**Cp**	**I**
0.662	0.304	0.051	0.003	0.002	0.707	0.327	0.058	0.001
0.392	0.082	0.022	0.002	0.001	0.473	0.071	0.022	0.000
Post-BD								
aRIC					***eRIC***			
Rp	**Rc**	**Cp**	**Ce**	**I**	**Rp**	**Rc**	**Cp**	**I**
0.308	0.315	0.111	0.003	0.001	0.393	0.268	0.125	0.001
0.123	0.134	0.075	0.005	0.001	0.146	0.063	0.067	0.000
Percent Change (%)								
aRIC					***eRIC***			
Rp	**Rc**	**Cp**	**Ce**	**I**	**Rp**	**Rc**	**Cp**	**I**
-53.5	3.7	119.7	19.2	-13.9	-44.3	-18.1	113.9	-4.2

Table 9-10: Estimated models' parameters for SAI subjects with pre and post-BD IOS measurements. The percent change for each parameter is included.

ESTIMATED PARAMETERS - SAI								
Pre-BD								
aRIC					***eRIC***			
Rp	**Rc**	**Cp**	**Ce**	**I**	**Rp**	**Rc**	**Cp**	**I**
0.560	0.355	0.051	0.002	0.002	0.580	0.396	0.059	0.001
0.146	0.113	0.029	0.002	0.001	0.176	0.087	0.025	0.000
Post-BD								
aRIC					***eRIC***			
Rp	**Rc**	**Cp**	**Ce**	**I**	**Rp**	**Rc**	**Cp**	**I**
0.458	0.322	0.069	0.002	0.002	0.461	0.358	0.079	0.001
0.152	0.124	0.040	0.002	0.001	0.156	0.105	0.035	0.000
Percent Change (%)								
aRIC					***eRIC***			
Rp	**Rc**	**Cp**	**Ce**	**I**	**Rp**	**Rc**	**Cp**	**I**
-18.1	-9.2	34.1	-9.9	-14.8	-20.6	-9.5	34.5	-10.0

9.4 MODEL PARAMETERS DISCRIMINATE BETWEEN HEALTH AND DISEASE

Parameters obtained using the aRIC and eRIC models of human respiratory impedance show a close correspondence with IOS indices and a greater sensitivity to bronchodilator administration. Moreover, estimated parameters differ between normal and diseased lungs in a sensible manner. The close correspondence between model estimates of C_p is also seen in BD response, as it reacts to treatment very similarly in both models. Tables Table 9-11 and

Table 9-12 show that for both models calculated C_p differs greatly between NL and ASTH, as well as NL and SAI. In the case of the aRIC model, R_p values are also very reasonable, they distinguish between normal and abnormal airways in all cases and react to BD treatment much like peripheral airways would. For the eRIC model, R_p does not perform nearly as well: it fails to distinguish between NL and ASTH subjects and its average value is higher in normal lungs than in those diagnosed with peripheral airway obstruction. The R_c parameter is not expected to distinguish between NL and other subjects because it simulates upper (central) airway resistance, which is not nearly as affected by the lung diseases studied here. So the fact that it fails to discriminate between health and disease can actually be considered as a positive, much in the same way as its insensitivity to BD treatment. In the aRIC model, R_c behaves as expected, but in the eRIC model, it differs significantly between NL and ASTH subjects but not between NL and SAI subjects, so its behavior is inconsistent and not very realistic.

Table 9-11: Statistical significance of the difference between calculated model parameters for NL and ASTH subjects.

Statistical Difference of Model Parameters for Normal and Asthmatic Subjects												
	aRIC						***eRIC***					
	NL Cp	**Asth Cp**	**NL Rp**	**Asth Rp**	**NL Rc**	**Asth Rc**	**NL Cp**	**Asth Cp**	**NL Rp**	**Asth Rp**	**NL Rc**	**Asth Rc**
Mean	0.283	0.046	0.324	0.685	0.235	0.315	0.303	0.055	0.787	0.747	0.249	0.344
p -value	**< 0.05**		**< 0.05**		> 0.05		**< 0.05**		> 0.05		**< 0.05**	

Table 9-12: Statistical significance of the difference between calculated model parameters for NL and ASTH subjects.

Statistical Difference of Model Parameters for Normal and SAI Subjects												
	aRIC						*eRIC*					
	NL Cp	**SAI Cp**	**NL Rp**	**SAI Rp**	**NL Rc**	**SAI Rc**	**NL Cp**	**SAI Cp**	**NL Rp**	**SAI Rp**	**NL Rc**	**SAI Rc**
Mean	0.283	0.143	0.324	0.449	0.235	0.322	0.303	0.152	0.787	0.526	0.249	0.299
p -value	**< 0.05**		**< 0.05**		> 0.05		**< 0.05**		**< 0.05**		> 0.05	

Chapter 10: CONCLUSIONS

The purpose of this thesis is two-fold: determine the best human respiratory impedance model for use with IOS data and establish the diagnostic relevance of that model's estimated parameters. Mead's model of respiratory impedance has been in use for some time and is well-established for use with FOT data; therefore it was initially the focus of this study. The model's drawback, its tendency to return physiologically unreasonable values for lung tissue (C_l) and chest wall compliance (C_w) when using IOS data, gave way to a thorough Laplace circuit analysis of the model hoping to better understand its behavior when subjected to IOS-like stimuli. The results of that investigation, that C_l and C_w have a mostly negligible effect in the circuit, validated the assumption that IOS excitation impulses produce a volume that is too low to stimulate the lung tissue and chest wall in the respiratory system. Previous publications had found that the two reductions of Mead's model, the aRIC and eRIC human respiratory impedance models, had good data fit for IOS data while producing parameter estimates that closely reflected IOS indices of SAI. Thus, the aRIC and eRIC models were selected as the focus of this research. An algorithm was developed to estimate model parameters using a nonlinear least-squares approach. The algorithm was developed and implemented in MATLAB and avoided local minima by using a large amount of random and unique initial conditions.

A very large database was collected over several years from several sources. This made the collected data very varied demographically, with subjects from the US, Australia, Sweden and the UK; ranging from children to older adults. In spite of this variety, data quality is very high and successfully focuses on either normal subjects or those that have peripheral airway disease. The data collection resulted in 670 total unique IOS measurements which were then used to calculate impedance model parameters by deploying the developed algorithm. Both the aRIC and eRIC models were found to provide very good data fit, with similar errors and nearly indistinguishable regressions. And so, efficiency of data fit was not a determining factor in selecting the best respiratory impedance model for IOS data.

Spirometry does not produce reliable indices of small airway impairment while IOS indices R5, fdR and AX have already been shown to be sensitive measures of small airway impairment. So those IOS indices are of special interest in this investigation. Here, previous findings were corroborated using an unusually large database, as it was found that those IOS parameters efficiently discriminate between patients classified as either normal, asthmatic or small airway impaired. Furthermore the availability of 408 normal adults (height: 180.3 cm ± 6.2 cm, age: 43.9 years ± 8.3 years) allows this thesis to establish a useful standard of normal IOS indices, which is seen in table 10-1. The average values found for SAI (which were closer to NL than those found for ASTH) were found to be at least 2 standard deviations larger than those found for normal subjects, which leads to the conclusion that these values are reliable for normal adult subjects.

Table 10-1: Normal values for IOS indices of respiratory function, mean and standard deviation.

NORMAL VALUES FOR IOS INDICES OF RESPIRATORY FUNCTION			
	AX	***fdR***	***R5***
Mean	0.209	0.031	0.262
S.D.	±0.298	±0.034	±0.080

10.1 CONCLUSION

Calculated parameter values for both the aRIC and eRIC models were found to closely relate to IOS indices, C_p in particular was found to be consistent between the two models and best relates to AX and fdR. Moreover, it was found to be more sensitive to BD treatment than any IOS-derived parameter. In the case of aRIC R_p, it was found that it too was a sensible measure of the respiratory system's response to BD administration. Not only because of its significant difference from pre to post-BD administration, but because it reacts in a manner that makes physiological sense, it reflects the expected decrease in peripheral airway resistance.

Table 10-2: Average and standard deviation of aRIC C_p and R_p as found in normal adult subjects.

NORMAL VALUES FOR aRIC PARAMETERS		
	Cp (l/kPa)	***Rp (kPa/l/s)***
Mean	0.283	0.324
S.D.	±0.258	±0.181

Table 10-3: Average and standard deviation of eRIC C_p and R_p as found in normal adult subjects.

NORMAL VALUES FOR eRIC Cp	
	Cp (l/kPa)
Mean	0.320
S.D.	±0.259

It was found that both models' calculated C_p discriminated healthy from diseased lungs in a significant manner, with aRIC R_p also being a reliable parameter. Normal values were therefore obtained using the previously mentioned 408 normal adults, the mean and standard deviation of those parameter values are shown in tables 10-2 and 10-3. Out of the three most significant model parameters eRIC C_p seems to be the best at distinguishing health from disease, being about .64 standard deviations larger than the mean value of eRIC C_p found for SAI subjects. In spite of their difference being statistically significant, mean values of aRIC R_p for NL and SAI subjects are too close for that parameter by itself to be considered reliable for diagnostic purposes, however, the availability of two parameters shown to reflect small airway impairment (aRIC C_p and R_p) can be advantageous.

The augmented-RIC model of human respiratory impedance offers slightly better data fit, a more realistic reaction to BD treatment, and provides two parameters shown to be reliable indices of small airway impairment. On the other hand, eRIC C_p by itself is the most reliable parameter in discriminating

normal from abnormal lung function. It's also worth noting that although aRIC R_c does not seem to be a relevant parameter in either normal or abnormal subjects, it does behave in a manner that makes physiological sense. Although R_c by itself offers no diagnostic value for small airway diseases it might still be possible that the aRIC model has three "reliable" parameters.

Table 10-4: Summary of results differentiating adult data from children data, values are reported as Mean ± S.D. Summary includes Demographics, IOS indices and estimated Model Parameters for both aRIC and eRIC. The summary excludes post-BD data. The p-values are with respect to NL of the same age group (adult or children) and a p-value < 0.05 is considered statistically significant.

SUMMARY OF RESULTS								
		Adults				Children		
		NL	ASTH	COPD	CF	NL	ASTH	COPD
Demographics	*No. of IOS Tests*	408	21	28	56	59	24	24
	Age (years)	43.9 ± 8.3	34.6 ± 9.4	43.9 ± 7.1	NA	17.4 ± 2.4	9.0 ± 2.4	9.7 ± 2.6
	Height (cm)	180.3 ± 6.2	170.1 ± 9.0	178.4 ± 6.3	169.2 ± 10.0	158.1 ± 17.4	130.5 ± 15.8	132.3 ± 16.0
IOS Indices	*AX (kPa/l)*	0.21 ± 0.30	2.37 ± 1.60	0.35 ± 0.49	0.72 ± 0.63	0.43 ± 0.50	2.26 ± 0.76	1.96 ± 0.85
	p-value		**< 0.001**	> 0.05	**< 0.001**		**< 0.001**	**< 0.001**
	fdR (kPa/l/s)	0.03 ± 0.03	0.26 ± 0.11	0.05 ± 0.06	0.11 ± 0.07	0.08 ± 0.07	0.29 ± 0.09	0.28 ± 0.10
	p-value		**< 0.001**	**< 0.05**	**< 0.001**		**< 0.001**	**< 0.001**
	R5 (kPa/l/s)	0.26 ± 0.08	0.60 ± 0.16	0.30 ± 0.10	0.40 ± 0.10	0.46 ± 0.12	0.68 ± 0.13	0.69 ± 0.13
	p-value		**< 0.001**	**< 0.05**	**< 0.001**		**< 0.001**	**< 0.001**
Model Parameters aRIC	*Rp (kPa/l/s)*	0.32 ± 0.18	0.71 ± 0.48	0.33 ± 0.17	0.44 ± 0.18	0.39 ± 0.14	0.67 ± 0.20	0.61 ± 0.19
	p-value		**< 0.001**	> 0.05	**< 0.001**		**< 0.001**	**< 0.001**
	Cp (l/kPa)	0.28 ± 0.26	0.06 ± 0.02	0.23 ± 0.09	0.14 ± 0.07	0.18 ± 0.08	0.04 ± 0.02	0.05 ± 0.03
	p-value		**< 0.001**	**< 0.01**	**< 0.001**		**< 0.001**	**< 0.001**
	Rc (kPa/l/s)	0.21 ± 0.06	0.31 ± 0.08	0.23 ± 0.06	0.28 ± 0.05	0.36 ± 0.09	0.30 ± 0.11	0.35 ± 0.11
	p-value		**< 0.001**	> 0.05	**< 0.001**		**< 0.01**	> 0.05
Model Parameters eRIC	*Rp (kPa/l/s)*	0.82 ± 0.68	0.76 ± 0.58	0.52 ± 0.43	0.48 ± 0.21	0.58 ± 0.46	0.73 ± 0.31	0.63 ± 0.22
	p-value		> 0.05	**< 0.001**	**< 0.001**		**< 0.05**	> 0.05
	Cp (l/kPa)	0.32 ± 0.26	0.06 ± 0.02	0.25 ± 0.10	0.14 ± 0.07	0.18 ± 0.08	0.05 ± 0.02	0.05 ± 0.02
	p-value		**< 0.001**	**< 0.01**	**< 0.001**		**< 0.001**	**< 0.001**
	Rc (kPa/l/s)	0.23 ± 0.06	0.32 ± 0.07	0.24 ± 0.05	0.29 ± 0.05	0.38 ± 0.08	0.36 ± 0.09	0.40 ± 0.08
	p-value		**< 0.001**	> 0.05	**< 0.001**		> 0.05	> 0.05

Table 10-4 shows a summary of results separating adult data from children data. In it, the p-values are calculated with respect to the NL data in the same age group (adult or children). In it one can see that C_p (for both models) is the best performing parameter in terms of differentiating from health from disease. In all cases it is able to discriminate normal from abnormal data and in a more statistically significant manner than even IOS indices. In general, aRIC performs slightly better than eRIC, aRIC R_p is able to distinguish health from disease in almost all cases and its mean values make more physiological sense than those for eRIC R_p. For pre-BD data, which is all that table 10-4 includes, both models' estimated R_c perform relatively well, although it is worth mentioning again that when comparing pre-BD to post-BD data aRIC R_c shows a realistic response to treatment.

The availability of more than one reliable parameter might be advantageous in computer-aided classification or in monitoring treatment response. Determining which model is more appropriate for use with IOS data might then be a matter of application. If one wished to use the model by itself as a diagnostic tool, then eRIC offers the better diagnostic parameter (eRIC C_p). By modeling IOS data using either aRIC or eRIC, parameters are obtained that are not only able to distinguish health from disease as well any other IOS parameter, but they offer valuable insight into the properties of specific regions in the lungs.

10.2 FUTURE WORK

The results obtained in this summary can be applied to improve current diagnostic capabilities of small airway disease. They might also be able to accurately diagnose a patient using computer-aided classification. Recently, it has been shown that IOS measured impedance shows a marked reaction to deep inspiratory maneuvers, in which a subject slowly inhales to full capacity and then slowly exhales (28). The stretching of airways due to the deep inspiration (DI) maneuver is measured by IOS a sudden drop in measured resistance immediately after DI,

followed by a slow steady increase as it approached impedance as measured before DI as shown in Figure 10-1 (28). Preliminary work shows that this maneuver might provide further insight into lung properties, as healthy and unhealthy subjects have distinct reactions in measured IOS indices as well as estimated model parameters. However, further research is needed in order to determine the best application of this maneuver and of the results obtained by using it.

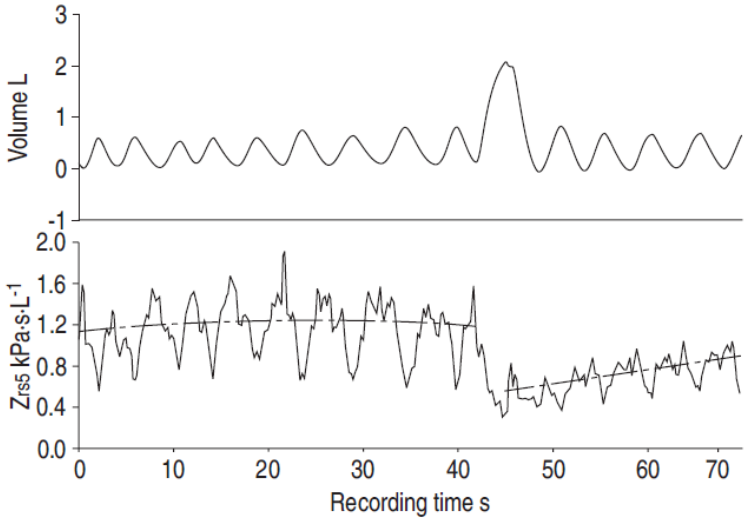

Figure 10-1: Tidal volume and magnitude of respiratory impedance at 5 Hz. First 40 s are resting breathing. After 40 s, subject inspired to total lung capacity, followed by relaxation back to normal resting breathing.

REFERENCES

1. **National Institutes of Health.** Lung Diseases. *Medline Plus.* [Online] US National Library of Medicine. [Cited: May 11, 2011.] http://www.nlm.nih.gov/medlineplus/lungdiseases.html#cat1.

2. **National Center for Health Statistics.** Asthma. *Center for Disease Control and Prevention.* [Online] [Cited: May 11, 2011.] http://www.cdc.gov/nchs/fastats/asthma.htm.

3. *Is forced expiratory volume in one second the best measure of severity in childhood asthma?* **J. D. Spahn, R. Cherniack, K. Paull and E. W. Gelfand.** 2004 , Am J Respir Crit Care Med, Vol. 169, pp. 784-786.

4. *Mechanical Properties of Lungs.* **Mead, J.** April 1961, Phys. Rev. , Vol. 41, pp. 281-330.

5. *Oscillation mechanics of lung and chest in man.* **A. B. DuBois, A. Brody, D. Lewis, B. Burgess.** 1956, J Appl Physiol.

6. *Physiological interpretations based on lumped element models fit to respiratory impedance data: Use of forward-inverse modeling.* **K.D., Lutchen K.R. and Costa.** 11, 1990, IEEE Trans. Biomed. Eng., Vol. 37, pp. 1076–1086.

7. *Computer simulation of the measured respiratory impedance in newborn infants and the effect of the measurement equipment.* **M. Schmidt, B. Foitzik, O. Hochmuth, and G. Schmalisch.** 3, 1998, Medical Eng. Physics, Vol. 20, pp. 220-228.

8. *Estimating Respiratory Mechanical Parameters in Parallel Compartment Models.* **Pimmel, J. Eyles and R. L.** 4, April 1981, IEEE Transactions on Biomedical Engineering, Vol. 28, pp. 313-317.

9. *Frequency response of the chest: Modeling and parameter estimation.* **R. Peslin, J. Papon, C. Duviver, and J. Richalet.** 4, 1975, J. Appl. Phys., Vol. 39, pp. 523-534.

10. *Modeling Human Respiratory Impedance.* **B. Diong, H. Nazeran, P. Nava, M. Goldman.** 1, 2007, IEEE Engineering in Medicine and Biology, Vol. 26, pp. 48-55.

11. *Transfer Impedance of the Respiratory System by Forced Oscillation Technique and Optoelectronic Plethysmography.* **A. Alivierti, R.L. Dellaca and A. Pedotti.** 2001, Annals of Biomedical Engineering, Vol. 29, pp. 71-82.

12. *Tracking variations in airway caliber by using total respiratory vs. airway resistance in healthy and asthmatic subjects.* **L. D. Black, R. Dellacà, K. Jung, H. Atileh, E. Israel, E. P. Ingenito and K. R. Lutchen.** April 11, 2003, Journal of Applied Physiology, Vol. 95, pp. 511-518.

13. *Assessment of bronchial reactivity by forced oscillation admittance avoids the upper airway artefact.* **R. Farre, M. Rotger, F. Marchal, R. Peslin and D. Navajas.** 1999, Eur. Respir. J. , Vol. 13, pp. 761-766.

14. *Resistance of the Intrathoracic Airways of Healthy Subjects During Periodic Flow.* **Finucane K., Dawson S., Phelan P., and Mead J.** 3, March 1975, Journal of Applied Physiology, Vol. 38, pp. 518-530.

15. *Relations Between Fractional-Order Model Parameters and Lung Pathology in Chronic Obstructive Pulmonary Disease.* **Keyser, C. Ionescu and R. De.** 4, April 1999, IEEE Transactions on Biomedical Engineering, Vol. 56, pp. 978 - 987.

16. *Reduction of a linear complex model for respiratory system during Airflow Interruption.* **Mroczka, I. Jabłoński and J.** Buenos Aires, Argentina : s.n., 2010. 32nd Annual International Conference of the IEEE EMBS. pp. 730-733.

17. **University of Stanford.** Respiratory System Summary. *Virtual Labs Media Library.* [Online] [Cited: May 5, 2011.] http://medialibrary.stanford.edu/medias/image/respiratory/resp.anatomy-intro,labeled.jpg.

18. **Rhoades R, and Pflanzer R.** *Human Physiology.* s.l. : Thomson, Brooks/Cole, 2003.

19. **University of Pennsylvania.** Lung Injury Research. *Injury Biomechanics Lab.* [Online] [Cited: May 10, 2011.] http://www.seas.upenn.edu/~injury/LungInjury.html.

20. [Online] [Cited: May 11, 2011.] http://retraitemutualisteducombattant.fr/gaseous-exchange-in-lungs.

21. **Guyton A., Hall J.** *Textbook of Medical Physiology, 11th Edition.* Philadelphia, Pennsylvania : Elseiver Saunders, 2006.

22. *Pulmonary function testing prior to hematopoietic stem cell transplantation.* **J W Chien, D K Madtes and J G Clark.** 2005, Bone Marrow Transplantation, Vol. 35, pp. 429–435.

23. *The small airways and distal lung compartment in asthma and COPD: a time for reappraisal.* **M. Contoli, J. Bousquet, L. Fabbri, H. Magnussen, K. Rabe, N. Siafakas, Q. Hamid and M. Kraft.** 2010, Allergy, Vol. 65, pp. 141-151.

24. *Relationship between Small Airway Function and Health Status, Dyspnea and Disease Control in Asthma.* **T. Takeda, T. Oga, A. Niimi, H. Matsumoto, I. Ito, M. Yamaguchi et al.** September 22, 2009, Respiration.

25. *Impulse oscillometry versus spirometry in a long-term study of controller therapy for pediatric asthma.* **G. Larsen, W. Morgan and G. Heldt.** 2009, J Allergy Clin Immunol, Vol. 123, pp. 861-867.

26. *Effect of inhaled corticosteroids on small airways in asthma: investigation using impulse oscillometry.* **M. Yamaguchi, A. Niimi, T. Ueda, M. Takemura, H. Matsuoka, M. Jinnai et al.** 2009, Pulm Pharmacol Ther., Vol. 22, pp. 326-332.

27. *Comparison of Effectiveness in Ciclesonide and Fluticasone Propionate on Small Airway Function in Mild Asthma.* **Hoshino, M.** 2010, Allergol Int., Vol. 59, pp. 59-66.

28. *Analysis of Impulse Oscillometric Measures of Lung Function and Respiratory System Model Parameters in Small Airway-Impaired and Healthy Children over a 2-year Period.* **Erika H. Meraz, Homer Nazeran, Carlos D. Ramos, Pat Nava, Bill Diong, Michael D. Goldman.** Biomedical Engineering Online Journal.

29. *IOS-based Model of Human Respiratory Impedance Tracks Small Airway Function in Health and Disease.* **H. Nazeran, C. Ramos, E. Meraz, N. Hafezi, P. Gustafsson, and M. D. Goldman.** Dallas, TX : s.n., 2011. Proceedings of 27th Southern Biomedical Engineering Conference.

30. *Electrical Circuit Models of the Human Respiratory System Reflect Small Airway Impairment Measured by Impulse Oscillation (IOS).* **M.D. Goldman, H. Nazeran, C. Ramos, Emily Toon, Katrina Oates, Diana Bilton, Erika Meraz, Nazila Hafezi and B. Diong.** Buenos Aires, Argentina : s.n. 2010 Annual International Conference of the IEEE Engineering in Medicine and Biology Society (EMBC). pp. 2467 - 2472 .

31. *Estimating Respiratory Mechanics with Constant-Phase Models in Healthy Lungs from Forced Oscillation Measurements.* **Ionescu C., Desager K., De Keyser R.** 1, 2009, Studia Universitatis "Vasile Goldiş", Vol. 19, pp. 123-131.

32. *The forced oscillation technique in clinical practice: methodology, recommendations and future developments.* **E. Oostveen, D. MacLeod, H. Lorino, R. Farre, Z. Hantos, K. Desager, and F. Marchal.** 2003, European Respiratory Journal, Vol. 22, pp. 1026–1041.

33. **E., Marieb.** *Human Anatomy & Physiology.* California : Pearson Benjamin Cummings, 2004.

34. *Resistance of central and peripheral airways measured by rethrograde catheter.* **P.T. Macklem, J. Mead.** 1967, J Appl Physiol, Vol. 22, pp. 395-401.

35. **National Institues of Health.** What is asthma? *National Heart Lung and Blood Institute.* [Online] [Cited: May 11, 2011.] http://www.nhlbi.nih.gov/health/dci/Diseases/Asthma/Asthma_WhatIs.html.

36. *Forced oscillation technique and impulse oscillometry.* **H. Smith, P. Reinhold, M. Goldman.** 2005, Eur. Respir. Mon., Vol. 31, pp. 72-105.

37. **Peslin R, Fredberg J.** Oscillation mechanics of the respiratory system. [book auth.] Mead J, eds. Macklem P. *Handbook of Physiology.* s.l. : American Physiological Society, 1986, Vol. III, Section 3, pp. 145–166.

38. *Respiratory impedance measured with a head generador to minimize upper airway shunt.* **R. Peslin, C. Duvivier, J. Didelon, C. Gallina.** 1985, J Appl Physiol, Vol. 59, pp. 1790-1795.

39. *Effect of upper airway shunt and series properties on respiratory impedance measurements.* **M. Cauberghs, K. P. Van de Woestijne.** 5, 1989, J Appl Physiol., Vol. 66, pp. 2274-2279.

40. *Changes of respiratory input impedance during breathing in humans.* **M. Cauberghs, K. P. Van de Woestijne.** 6, 1992, J Appl Physiol., Vol. 73, pp. 2355-2362.

41. *Electrical Circuit Models of the Human Respiratory System Reflect Small Airway Impairment Measured by Impulse Oscillation (IOS).* **M.D. Goldman, H. Nazeran, C. Ramos, Emily Toon, Katrina Oates, Diana Bilton, Erika Meraz, Nazila Hafezi and B. Diong.** Buenos Aires, Argentina : s.n., 2010. Proceedings of the IEEE EMBS 32nd Annual International Conference.

42. *Respiratory Symptoms and Physiologic Assessment of Ironworkers at the World Trade Center Disaster Site.* **G. Skloot, M. Goldman, D. Fischler, C. Goldman, C. Schechter, S. Levin, et al.** 2004, Chest, Vol. 125, pp. 1248-1255.

43. *Circuit Analysis Justifies a Rduced Mead's Model of the Human Respiratory Impedance for Impulse Oscillometry Data.* **C. Ramos, H. Nazeran, M.D. Goldman, B. Diong.** Buenos Aires, Argentina : s.n., 2010. Proceedings of the IEEE EMBS 32nd Annual International Conference.

44. *Diagnostic Utility of a Reduced IOS-based Mead's Model of the Human Respiratory System Impedance in Health and Disease.* **Carlos Ramos, Homer Nazeran and Michael D. Goldman.** Arlington, TX : s.n., 2011. 27th Southern Biomedical Engineering Conference .

45. *The Augmented RIC Model of the Human Respiratory System.* **B. Diong, A. Rajagiri, M. Goldman, H. Nazeran.** 2009, J Med Biol Eng Comp, Vol. 47, pp. 395-404.

46. *Physiological Interpretations Based on Lumped Element Models Fit to Respiratory Impedance Data: Use of Forward-Inverse Modeling.* **COSTA, KENNETH R. LUTCHEN AND KEVIN D.** 11, 1990, IEEE TRANSACTIONS ON BIOMEDICAL ENGINEERING, Vol. 37, pp. 1076-1086.

47. *Contribution of compliance of airways to frequency-dependent behavior of lungs.* **Mead, J.** 5, May 1969, Journal of Applied Physiology, Vol. 25.

48. *Impulse Oscillometric Features of Lung Function: Towards Computer-Aided Classification of Respiratory Diseases in Children.* **Meraz E, Nazeran H, Goldman M, Nava P, Diong B.** Vancouver, Canada : s.n., 2008. Proceedings of the IEEE EMBS. pp. 2443-2446.

49. *Modeling Human Respiratory Impedance in Hispanic Asthmatic Children.* **Meraz E., Nazeran H., Diong B., Menendez R., Ortiz G., Goldman M.** 2001. Annual International Conference of the IEEE EMBS.

50. *Clinical Applications of Forced Oscillation to Assess Perhiperal Airway Function.* **M. Goldman, C. Saadeh, D. Ross.** 2005, Res Physiol Neuro, Vol. 148, pp. 179-194.

51. *Direct Assessment of Small Airways Reactivity in Human Subjects.* **ELIZABETH M. WAGNER, EUGENE R. BLEECKER, SOLBERT PERMUTT, and MARK C. LIU.** 2, 1998, Am. J. Respir. Crit. Care Med., Vol. 157, pp. 447-452.

CURRICULUM VITA

Carlos Ramos Rocha was born in Ciudad Juarez, Mexico. The third child of Dr. Arturo Ramos and Dr. Bertha Rocha, he coursed his high school studies at the Instituto Tecnologico y de Estudios Superiores de Monterrey at his hometown. He began his college-level studies at the El Paso Community College and transferred to the University of Texas at El Paso (UTEP) after completing most of his lower-division coursework, where for his Senior Project he participated in the design and development of a vision-based robotic arm manipulator. During his last semester of undergraduate studies he started working as both a Research Assistant and Teaching Assistant in the Biomedical Engineering laboratory, a job he kept throughout his graduate studies as well.

During his graduate studies at UTEP he worked as a teaching assistant, developing and supervising laboratory coursework for two graduate-level biomedical engineering classes. As a Research Assistant his work with Impulse Oscillometry led to two publications in the IEEE EMBS conference and two more in the Southern Biomedical Engineering Conference as well as one publication in the Biomedical Engineering Online Journal. He also worked during the summers of 2009, 2010 and 2011 as a mentor for high school students in the Transmountain Early College High School program, supervising research projects in the biomedical engineering field.

Permanent address: 649 Madrigal Rd.,
Socorro, TX, 79927